# UNIVERSITA' DEGLI STUDI DI PADOVA


Dipartimento di Ingegneria Industriale – DII

Corso di Laurea Magistrale in Ingegneria Meccanica

Master Thesis

# DESIGN OF A VIBRATION ISOLATION SYSTEM FOR REDUCING THE VIBRATION LEVEL IN A MOBILE ROBOT

**Relatore**: Prof. Maria Elena Valcher

**Co-relatori**: Prof. J. Martínez

Prof. Mª A. de los Santos

**Laureando**: Andrea Parise

2015/2016

# Abstract

This thesis focuses on the problem of passive vibration isolation applied to a mobile robot. The goals of the project are to analyse the disturbances that affect the mobile robot and to develop a passive vibration isolation system as solution to this problem.

Once the mobile robot will be presented, experimental measurements will be executed to estimate the main frequencies of the disturbance and the mobile robot during its motion, analysing the configurations with the higher vibration level.

A theoretical model will be implemented in order to describe the behaviour of the mobile robot and the isolation system will be designed. Special attention will be paid to the stability problems, analysing also the responses of the mobile robot to different acceleration inputs.

The displacements caused by inertia effects will be limited by the introduction of a clamping system that blocks the deflections of the mobile robot during transient motions and during the robot arms' activities. Then, kineto-static simulations will be run in order to determine the static forces acting on the members of the mechanism.

Finally, the precision of the theoretical model will be verified by experimental measurements.

Experimental results will be compared with theoretical results in order to understand which are the configurations that better fit the theoretical model and also to estimate the margin of error of the model that ensures a good attenuation of the vibrational phenomena and the correct behaviour of the mobile robot during its motion.

# Contents

# Introduction

Robotics has reached its greatest achievements to date in the world of industrial manufacturing. Fixed at its shoulder to a specific position in the assembly line, the robot arm can move with great speed and accuracy to perform repetitive tasks such as spot welding and pick & place operations. This type of technology is used in different industrial fields such as the electronics industry where it can place surface-mounted components with great precision or in the mechanic industry to assemble super complex machines.

For all of their successes, these commercial robots suffer from a fundamental disadvantage: lack of mobility. Fixed manipulators have a limited range of motion depending on where they are fixed. Robot manipulators are usually considered as rigid multi-body mechanical systems. This ideal assumption simplifies dynamic and cinematic analysis and control design, but may lead to performance degradation due to the excitation of vibrational phenomena. Heavy machines that act nearby the assembly line can generate vibrations and cause loss of accuracy: it is often recommended not to place assembly lines next to them.

There are several types of robots on the market and their on-going development will bring many new applications. Underwater robots are already used to explore oceans; wheeled robots can be used to explore planets, and drones are used for monitoring wide areas: these are all tasks that require successful execution without human direct supervision. Robots as the ones described above are called mobile robots and they can be used inside the factories because they are able to move throughout the manufacturing plant and complete complex operations.

The original project, developed by the “Institut d’Organitzaciò i Control de Sistemes Industrials” (IOC), was the realization of an omnidirectional mobile platform with a “lightweight 4” by Kuka Robot bolted on it. To this purpose, IOC appointed the group of “Disseny de Màquines”, belonging to the Mechanical Engineering Department, to design and realise the platform.

The mobile robot is therefore the result of the composition of a wheeled robot and a manipulator robot arms. The combination of these two features guarantees great flexibility to the system and allows the cooperation between the two manipulators and with other apparatuses to accomplish complex manipulations.

As previously said, having a good working area in which robots can accomplish their tasks is an important factor that has to be considered in order to let them perform at their best, but this is not always possible. Pavement flaws, electric wires, obstacles and little steps can influence negatively the behaviour of mobile robots during their motion inside the factory because of vibrations generation.

This thesis focuses on the study of vibration problems that affect this type of machines. The main goal is to develop and design a vibration isolation system in order to reduce the vibration level in

mobile robots. Secondary aspects, as cost analysis and environment impact, are examined in order to study the subject with a holistic approach.

The thesis is structured in nine chapters.

The first chapter is the presentation of the mobile robot. Technical specifications, geometry of the system, description of the omnidirectional wheels, arrangement of motor groups and choice of the electric motors are the principal information that help understanding the global architecture of the system.

The second chapter is about the laboratory measurements and experimental acquisition. The laboratory tests focus on the estimation of the main frequency of the disturbance and the wideness of the frequency spectrum.

The third and fourth chapters pertain the study of vibrations: theoretical analysis of one degree of freedom system, typical response of two degrees of freedom systems and choice of the stiffness for the mobile robot are the main topics.

In the fifth and sixth chapters, the rolling vibration of the machine is studied and the description of possible solutions for a clamping system that blocks the vertical displacement of the platform during transient motion are given. The analysis and the kineto-static simulation of toggle mechanism are shown.

In the seventh chapter, the accuracy of the theoretical model is verified through experimental measurements. The solution proposed is installed and several configurations and joints' states are tested. The aims of the measurements are to determine the margin of error of the theoretical model in contrast to the experimental results.

In the eighth and ninth chapters, the environmental impact and budget evaluation of the project are presented.

# 1. Architecture of the mobile robot

The architecture of the mobile robot is conceived to be simple and functional. It is the result of several compromises between performances, dimensions and costs. In this chapter, the main characteristics of the mobile robot are described. Starting from the technical specifications defined by the IOC, the attention is focused on the type of omnidirectional wheels, the disposition of motor groups on the platform and the choice of the electric motors and adapters.

## 1.1. Technical specifications

The definition of the technical specifications is the very first step of the project. Here, the maximum performances of the platform are specified and the global complexity of the system is determined.

Since the mobile robot has to be omnidirectional, it implies three degrees of freedom in plane are required and these are translations along x-axis and y-axis and rotation around z-axis.

The accuracy of positioning, depending on rotation angles of the omnidirectional wheels, has to be extremely precise in order to guarantee good repeatability.

The maximum longitudinal and transversal velocities have to be $1\ {}^{m}/_{s}$ and the maximum longitudinal and transversal accelerations have to be $1\ {}^{m}/_{s^2}$.

The maximum rotational velocity is $3{,}14\ {}^{rad}/_{s}$ and the rotation acceleration $2\ {}^{rad}/_{s^2}$.

The dimension of the platform has to be small enough to pass through laboratory gates and office doors, and big enough to carry all the instrumentations such as motor drivers, controllers, manipulators, and other auxiliary elements. Good distribution of the mass on the platform has to be achieved.

The last technical specification is the most important for the development of this thesis: the ability to overcome obstacles of height up to $10\ mm,$ like wires and pavement flaws, is required.

The ability to overcome obstacles makes the mobile robot more autonomous during its motion, but impulsive bumps generate a wide spectrum of frequencies from low to high passing through resonance.

## 1.2. Geometry of the system

The second part of the project consists in the definition of the conceptual design of the mobile robot. It is composed by the platform, the 'T-shape' structure that holds the two robot arms, and the two manipulators UR5, as displayed in Figure 1.1.

The dimensions of platform and structure, the choice of the type of omnidirectional wheels, the number and the arrangement of the motor groups, the definition of the transmission and the choice of the electrical motors are the main aspects that have to be defined.

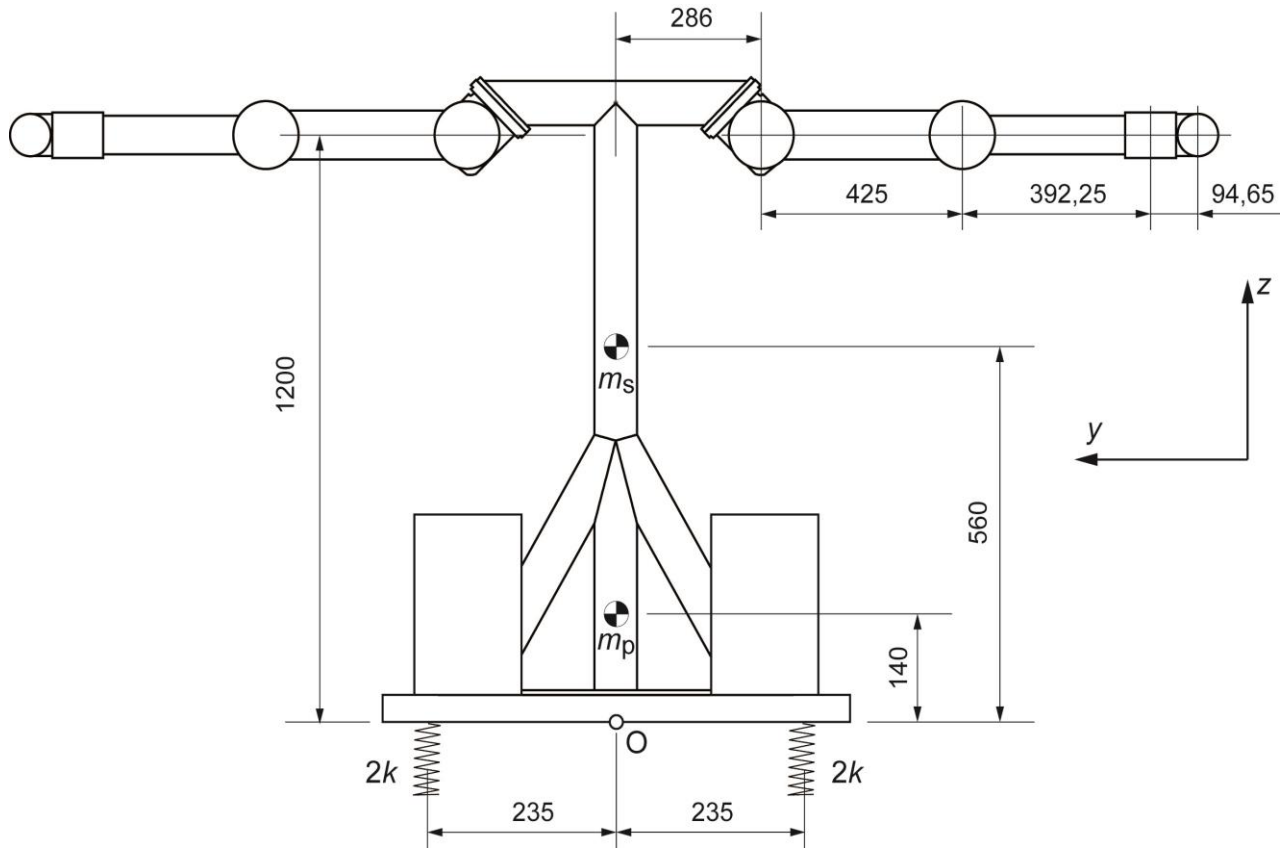


***Figure 1.1**: Representation of the mobile robot. From bottom to top, there are the platform with the isolation system and the controllers of the manipulators, the 'T-shape' structure and the two manipulators.*

### 1.2.1. Platform

The platform is the subsystem that generates the motion of the mobile robot. It is provided with omnidirectional wheels, an isolation system and auxiliary components.

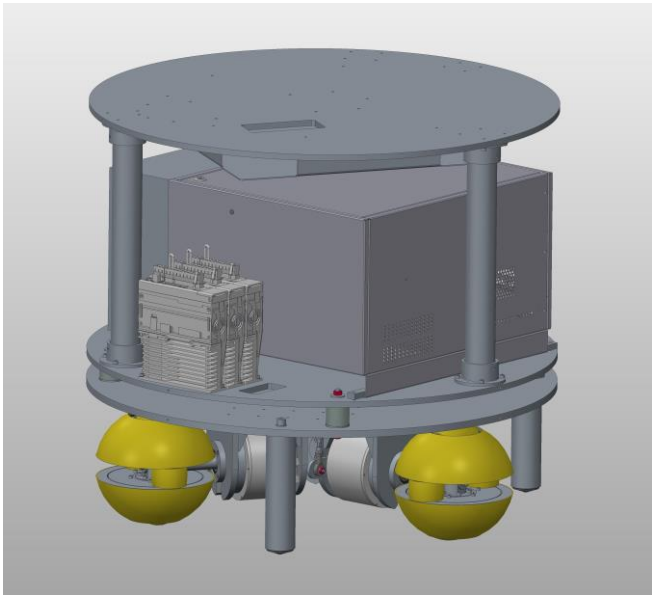

***Figure 1.2**: Circular platform with controllers, omnidirectional wheels and motor groups.*

The first choice is to use a circular platform with a diameter of 780 millimetres. The choice of the number of motor groups to place on the platform is made considering the optimization of space.
Circular shape allows to place three motor groups, and their control system devices, in an equilateral triangle arrangement. Moreover, the implementation of control equations of the platform with three motor groups is easier than the one with four motor groups, although the stability of the system would be enhanced.

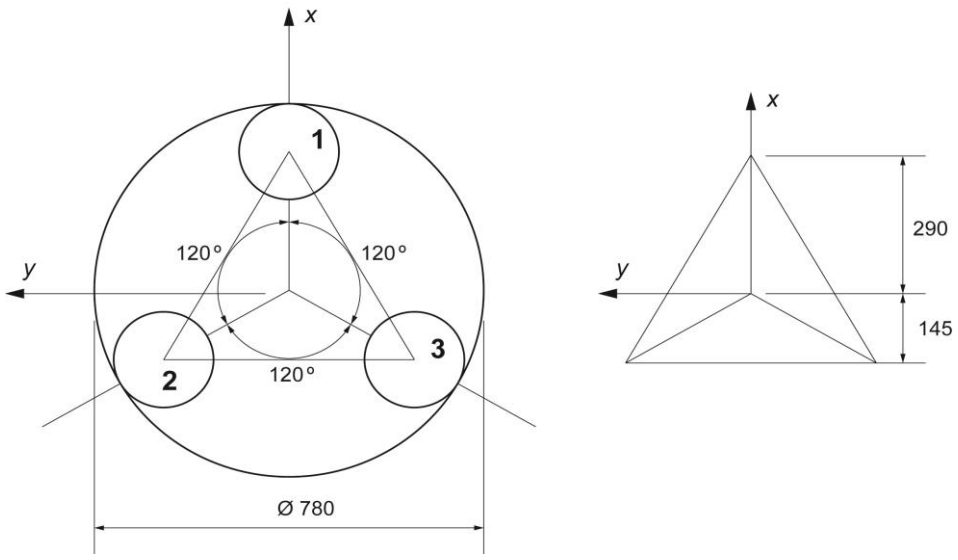


***Figure 1.3**: Geometry of the platform and disposition of the three motor groups.*

### 1.2.2. T-shape structure

The ‘T-shape’ structure is bolted on the bottom to the platform and on the top to the manipulators UR5. The tubular sections are hollow and connected by welded joints. The geometrical dimensions are represented in the Figure 1.4.

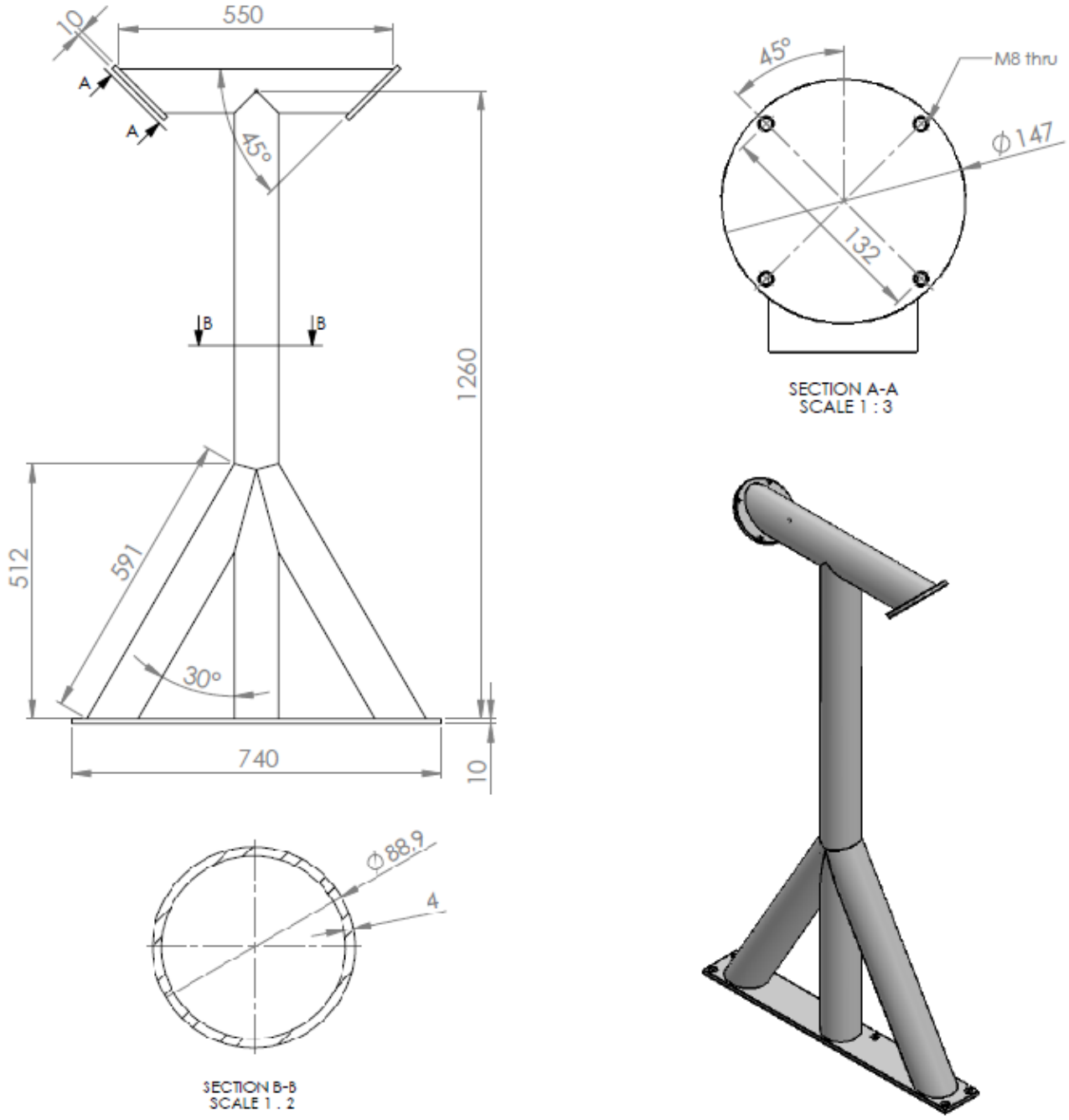


***Figure 1.4**: Geometrical details of the structure. Quotations and isometric view.*

### 1.2.3. Manipulators UR5

Two manipulators are fixed to the extremities of the ‘T-shaped’ structure. One has left arm configuration and the other right arm configuration.

UR5 from Universal Robots is a lightweight and flexible industrial robot and is a 6-axis manipulator with a working radius of $850\,mm$ and payload of up to $5\,kg$. The UR5 is ideal to optimize low-weight collaborative processes, such as picking, placing and testing. The aim of the robot is to complete complex manipulations though the cooperation of the two manipulators.

***Figure 1.5****: Universal Robot UR5* [7].

### 1.2.4. Position of the gravity centre

The mass of the elements are:

Platform (*p*): $m_p = 67$ kg,

Structure (s): $m_s = 25$ kg,

Manipulators (*m*): $m_m = 2 \cdot 18{,}4 = 36{,}8$ kg.

Total mass: $m = m_p + m_s + m_m = 128{,}8$ kg.

The distances between the centre of the platform *O* and each inertia centre are:

$d_p = 140$ mm,

$d_s = 560$ mm,

$d_m = 1200$ mm.

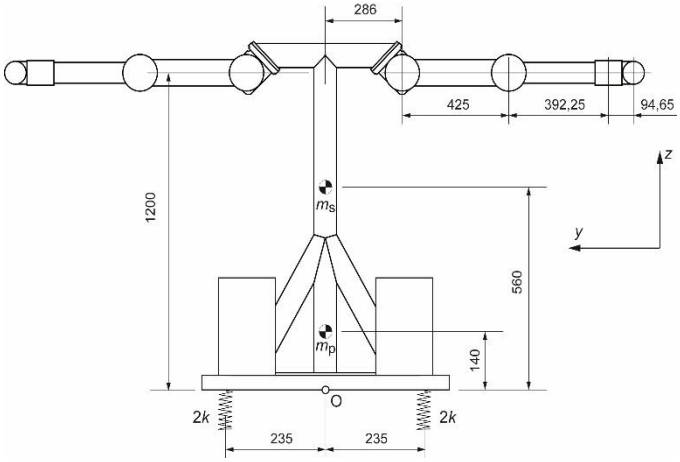


***Figure 1.6**: Configuration used to evaluate the gravity centre and the inertia moments of the mobile robot.*

Considering the configuration displayed in Figure 1.6 with both manipulators extended in horizontal position, the gravity centre is aligned with platform's and structure's gravity centres thanks to the symmetry of the configuration, so the position of the global gravity centre from the rotation point O is:

$$m\,h = m_p d_p + m_s d_s + m_m d_m$$

$$h = \frac{m_p d_p + m_s\, d_s + m_m d_m}{m} = \frac{67 \cdot 140 + 25 \cdot 560 + 36{,}8 \cdot 1200}{128{,}8} = 524 \text{ mm}$$

### 1.2.5. Estimation of inertia moments

The inertia moments of the mobile robot can be calculated considering the elements that compose it as cylinders. According to the reference system in Figure 1.6, the platform and the structure are z-axis oriented cylinders, while the manipulators in that configuration are y-axis cylinders.

The inertia moments of the three members referred to their own gravity centres are:

Platform: $I_{x,p}^G = I_{y,p}^G = 7\ \mathrm{kgm}^2$,

Structure: $I_{x,s}^G = I_{y,s}^G = 4{,}2\ \mathrm{kgm}^2$,

Manipulators:

$$I_{x,m}^G = \frac{1}{12} m_m (3r^2 + l^2) = 4{,}4\ \mathrm{kgm}^2$$

$$I_{y,m}^G = \frac{m\, r^2}{2} = 0{,}1\ \mathrm{kgm}^2$$

With $r = 74\ \mathrm{mm}$ and $l = 1200\ \mathrm{mm}$.

The inertia moment of the whole system with respect to the global gravity centre is calculated using the Huygens-Steiner theorem. $\delta$ is the distance between member's gravity centre and system's gravity centre. In particular:

$\delta_p = 524 - 140 = 384\ \mathrm{mm}$

$\delta_s = 560 - 524 = 36\ \mathrm{mm}$

$\delta_m = 1200 - 524 = 676\ \mathrm{mm}$

The inertia moments around x-axis $I_x^G$ and around y-axis $I_y^G$ are respectively:

$$I_x^G = I_{x,p}^G + m_p \delta_p^2 + I_{x,s}^G + m_p \delta_s^2 + I_{x,m}^G + m_m \delta_m^2 = 42{,}1\mathrm{kgm}^2$$

$$I_y^G = I_{y,p}^G + m_p \delta_p^2 + I_{y,s}^G + m_p \delta_s^2 + I_{y,m}^G + m_m \delta_m^2 = 37{,}8\mathrm{kgm}^2$$

## 1.3. Omnidirectional wheels

Using omnidirectional wheels, the platform is free to move in each direction conserving the three degrees of freedom in the space: the two linear translations along the x-axis and the y-axis, and the rotation around the z-axis. The composition of omnidirectional wheel is complex and is described below.

Small rollers are placed around the circumference of each wheel. Their orientation is perpendicular to the turning direction of the wheel and moreover they are free to roll around their axis. While wheels are driven with full force by a motor, rollers can roll at the same in the perpendicular direction. In this way, two different displacements in two perpendicular directions are possible.

With the combination of three omnidirectional wheels arranged in the correct position, the three degrees of freedom on plane are controlled and consequently the motion of the platform, too.

Three is the minimum number required for achieving complete omnidirectional motion. There are many different types of omnidirectional wheels, for example simple wheel, Mecanum wheel and Spherical wheel. In the Figure 1.7, Mecanum wheel and simple wheel are shown. The difference between them is the inclination of the free rotation axis, that is 45 degrees in Mecanum wheels and 90 degrees in simple wheels.

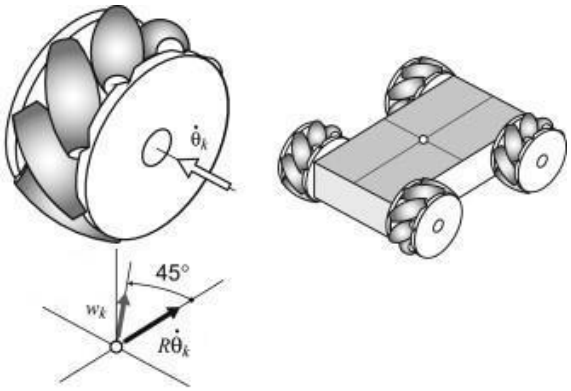


***Figure 1.7a**: Mecanum wheel* [3].

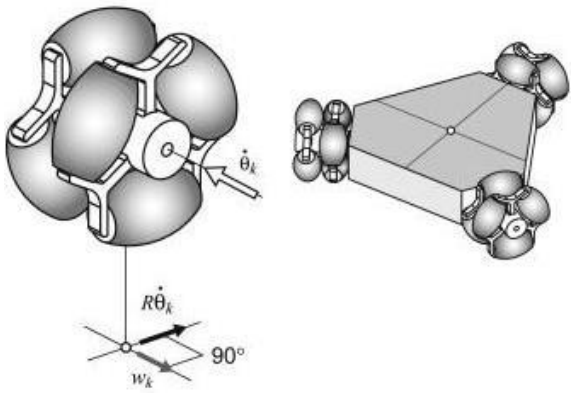


***Figure 1.7b**: Simple Omni wheel* [3].

The ones used in the mobile robot are spherical wheels and Figure 1.8a shows them. There are two spheres side by side. Each sphere is free to rotate around its polar axis. When the polar axis is in vertical position the rolling is not possible because polar regions are singular points that can only slide, thus the spheres are cut off at polar region. Two wheels are required because, when one is next to the polar region and loses the contact with the ground, the second one has to be fully in contact. These have 90 degrees difference of orientation in order to guarantee permanently the contact. The angle of truncation of polar regions is $< 90°$: in this way there is a little overlap between the two wheels in order to ensure one contact point permanently.

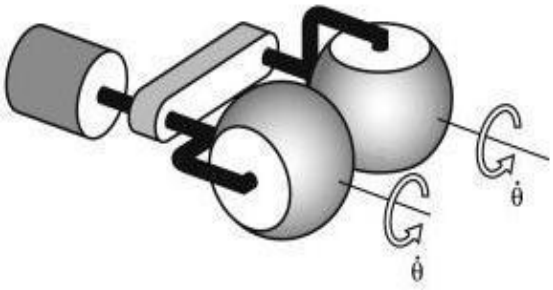

***Figure 1.8a**: Detail of the Omni wheel* [3].

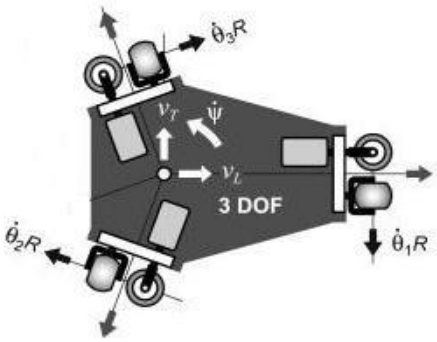


***Figure 1.8b**: Disposition of motor groups*

There are two possible solutions for assembling spherical wheels, described in the Figure1.9.
The first solution uses a wheel with a central gap in which the motor shaft is connected to the free rotational axis of the wheel. The second solution uses a fork connected to the free rotational axis by the two truncated extremities of the wheel.
The first solution introduces a little gap in the equatorial region of the wheel and during the motion of the platform such a discontinuity may produce vibrations, but does not affect the accuracy of the positioning. Instead in the second solution, when the orientation of the free rotational axis is vertical, the space between the fork and the soil is limited and the fork can interfere with obstacles making the positioning of the platform imprecise. Moreover the first solution is easier to build because the geometry of the fork is complex and difficult to be made, thus the first solution is adopted in this project.

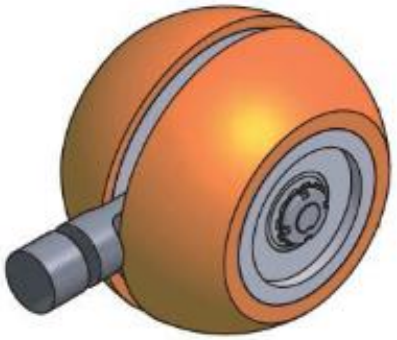

**a)**

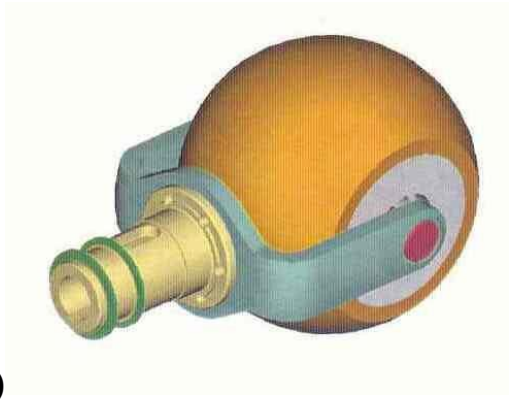

**b)**

***Figure 1.9a**: Solution with the central gap in which the motor shaft is connected to the free rotational axis* [1].
***Figure 1.9b**: Solution with the fork connected to the free rotational axis by the two truncated extremities* [1].

Spherical wheels present many advantages compared to peripheral rollers wheels as Mecanum wheel. Peripheral rollers wheels are constructively more complex than spherical wheels. It requires

a huge number of elements like rollers, shafts and bearings, but these are necessarily small because the available space is small and thus the weight they sustain is limited too. The spherical wheel is bigger and has bigger bearings, thus sustains a heavier weight.

Moreover, the more frequently the contact point changes, the less accurate the final position of the system is. Peripheral rollers wheel changes it every time a roller changes, it means more than ten times per cycle depending on the number of rollers that compose the wheel. Every time the contact roller changes, the terms of the Jacobian matrix of the platform change, because they depend on the distance between the frame origin and the contact point. In spherical wheels the contact point changes four time per cycle, but that distance do not change, so this kind of problem is not verified using spherical wheels.

The diameter of the sphere is 200 millimetres. It is large enough to overcome obstacles up to ten millimetres height and small enough to contain the torque that motor groups have to provide. Wheels are covered by thin elastomeric thickness that helps the grip.

## 1.4. Motor groups

The number and the position of the motor groups are aspects very important for the stability of the mobile robot. The best choice is to use four motor groups arranged in square to ensure better stability, but the problems of using redundant number of motor groups is that a suspension system or an articulated frame are required to get simultaneous contact of all the groups with the floor.

The disadvantages caused by a redundant number of motor groups are also related to space and costs. The required structure is more sturdy, control equations are more complex and the disturbances provoked by the changings of the points of contact of the wheels are higher, although there are more contact points so the system is more stable.

The platform has to carry the whole instrumentation as motor drivers, controllers, manipulators, and other auxiliary elements, thus the compromise solution is to arrange three motor groups in an equilateral triangle position. The control equations of the platform are simpler in this configuration, because three is the minimum number required to achieve complete omnidirectional motion.

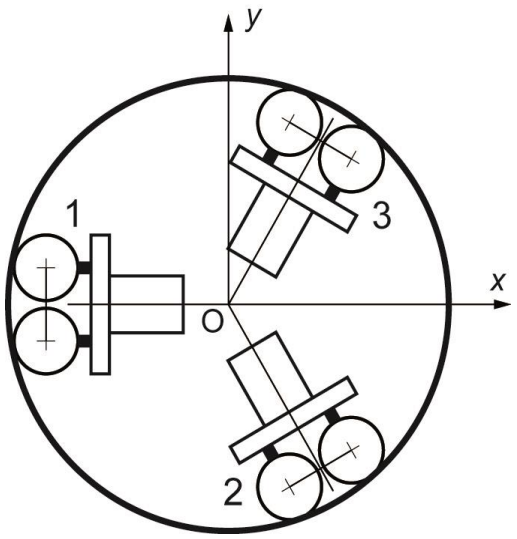


***Figure 1.10****: Disposition of the three motor groups on the circular platform* [1].

For these applications, electric motors are typically DC. Standard DC brushless motors are very flexible, but are characterized by high rotation velocity, thus they necessarily require adapters, usually reduced gearboxes, in order to reduce wheels velocity. These components have huge clearance that generates position errors in output shaft. There are adapters with very low clearance but they are expensive and require auxiliary elements to be fixed to the motor. For these reasons, motor groups are AC synchronous motors with controllers that adjust torque and velocity. The choice of synchronous motors is unusual but acceptable. In Figure 1.11, motor group, transmission and Omni wheels are represented.

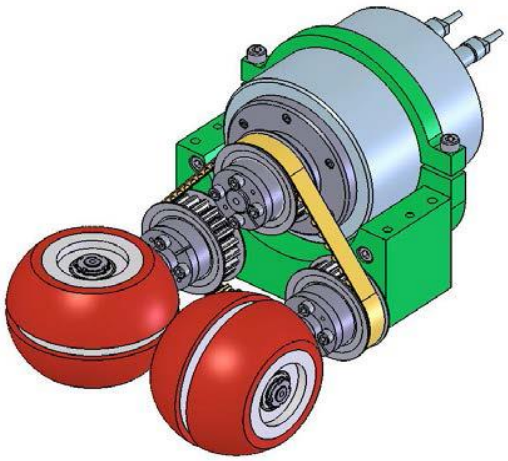

***Figure 1.11**: Motor group: AD synchronous motor, transmission and Omni wheels* [1].

AC Synchronous motors are characterized by low rotation velocity and high torque, thus they do not require adaptors. Position errors in output shaft are smaller, thus the accuracy of the motion is higher. Although they are expensive, the cost is similar to DC motor with low clearance adapter.

# 2. Experimental measurements

The aims of the tests are to estimate the main frequencies of the structure and also to analyse in which configurations the vibration level is higher. In this chapter, the execution of the tests is described and the laboratory equipment is presented. The acquired data are elaborated and the wide spectrum of frequency is evaluated. In the end, the corresponding cut-off frequencies are calculated to design the isolation system.

## 2.1. Execution of the tests

The experimental tests were conducted on November 27, 2015 in the laboratory of the Mechanical Engineering Department under the monitoring of operators and supervisors.

The aim was to estimate the main frequencies that affect the mobile robot during its motion on the pavement of the laboratory and to analyse in which configuration the vibration level is higher.

The mobile robot used for these tests is equipped with a rectangular platform instead of the circular one described in the previous chapter and it is not equipped with three omnidirectional wheels combined with motor groups, but with four conventional wheels.

These differences will not modify significantly the results, thus the frequencies obtained in tests with the rectangular platform can be considered similar to the ones obtained with the circular platform.

The measurements are obtained pushing and pulling the base of the mobile robot through the laboratory. The irregularities of the pavement reproduce a plausible estimate of the disturbances that may affect the motion of the mobile robot in different working environments.

Two configurations of the manipulators, displayed in Figure 2.2 and Figure 2.3, are set in order to analyse the different responses of the system. The first configuration tested is characterized by extended arms in transversal horizontal position and the second is characterized by folded arms in forward position.

Manipulators joints have internal brakes that allow to block all the joints for security reasons when the power is off. When powered, brakes are not active and electric motors control the position of the joints. Several measurements are conduct with power on -joints motors powered- and with power off -joints motors braked- in order to understand the influence of the stiffness of the joints.

The schedule of the tests is:

1) Extended arms in transvers horizontal position. Joint motors braked.
   Test 1° pushing
   Test 2° pulling
   Test 3° pushing

2) Extended arms in transverse horizontal position. Joint motors powered.
   Test 4° pushing
   Test 5° pulling
   Test 6° pushing

3) Folded arms in forward position. Joint motors powered.
   Test 7° pulling
   Test 8° pushing

4) Folded arms in forward position. Joint motors braked.
   Test 9° pulling
   Test 10° pushing

In Figure 2.1 the reference system adopted is displayed. The variable *z* is referred to as the vertical displacement along the z-axis and the variable $\vartheta$ is referred to as the rotation around the y-axis.

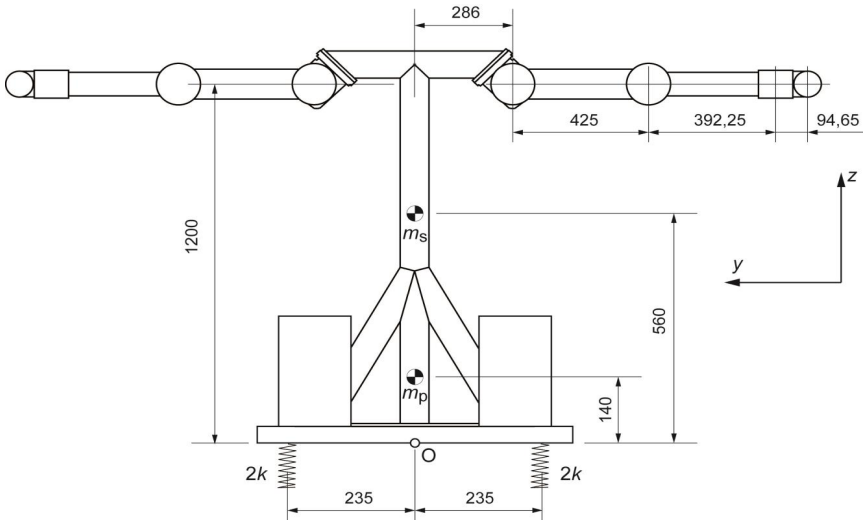


***Figure 2.1**: Reference system.*

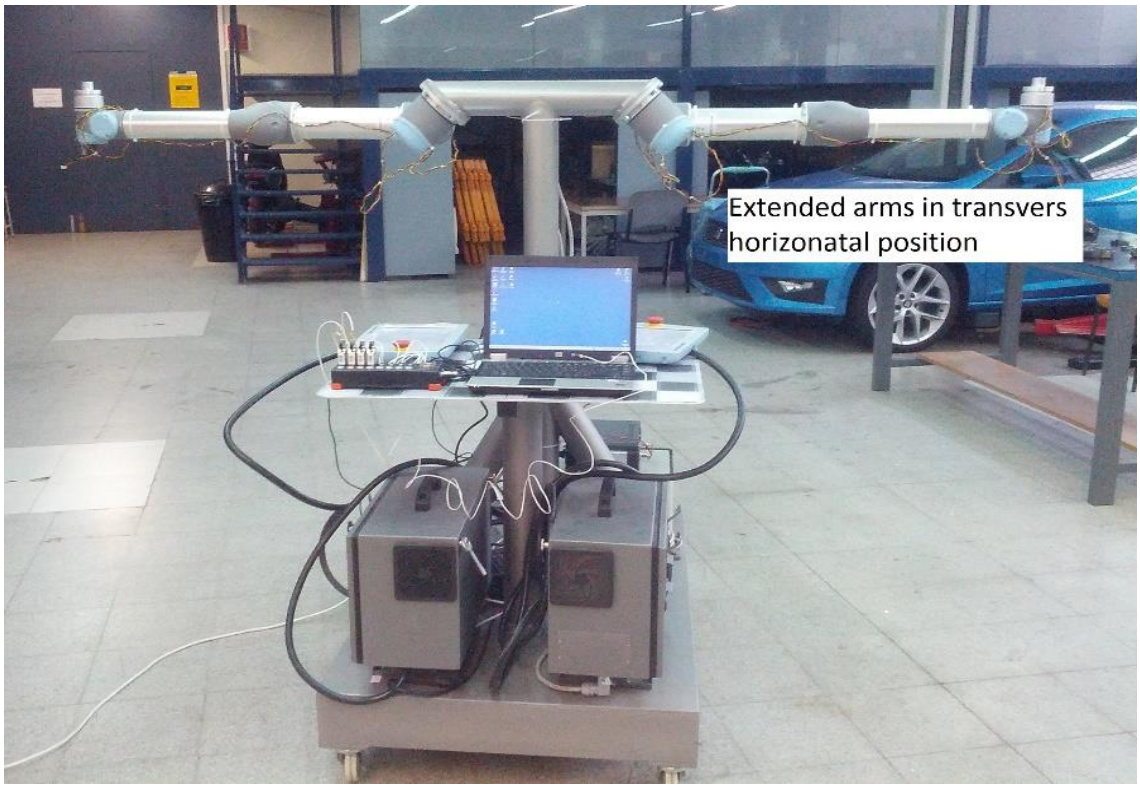


***Figure 2.2**: First configuration with extended arms in transvers horizontal position. In background, it is possible to see laboratory, pavement and equipment placed on the platform such as the acquisition instrumentations.*

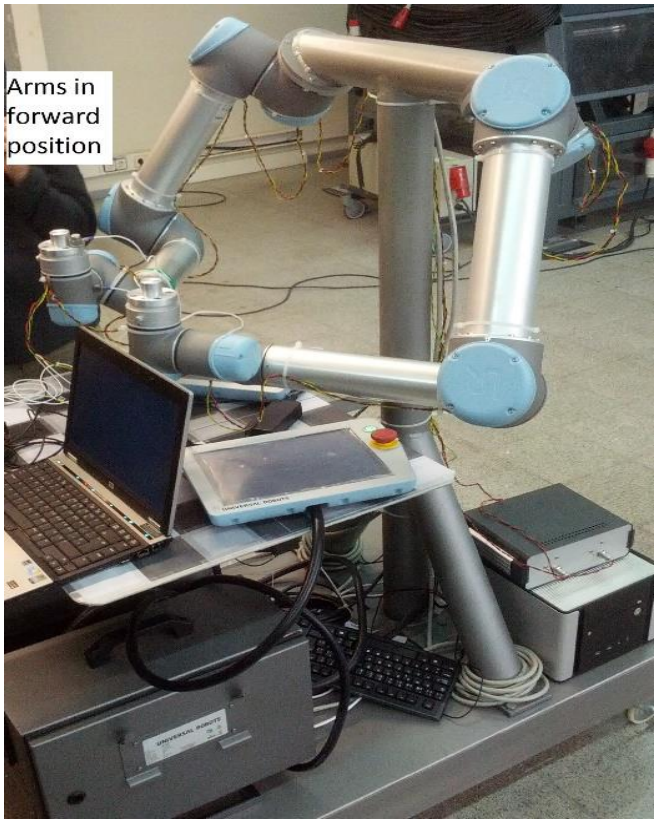


***Figure 2.3**: Second configuration with both arms folded in forward position. It is possible to see part of the equipment on the platform and the instrumentations used for the acquisition of the measurements.*

## 2.2. Laboratory equipment

The laboratory equipment is composed by two transducers, a data acquisition system and an HP laptop: they are described in Appendix 1.

The transducers are an *Accelerometer Endevco type 7254 A-10* and an *Accelerometer* Brüel & Kjær *type 4508*, and they acquire respectively the vibration accelerations along the y-axis and the x-axis.

Transducers:

Channel 0: *Accelerometer Endevco type 7254 A-10*,

Sensitivity of 1,016 $^{\mathrm{mV}}/_{\mathrm{ms^s}}$

Acquires vertical direction.

Channel 1: *Accelerometer* Brüel & Kjær *type 4508*,

Sensitivity of 9,985 $^{\mathrm{mV}}/_{\mathrm{ms^s}}$

Acquires horizontal direction.

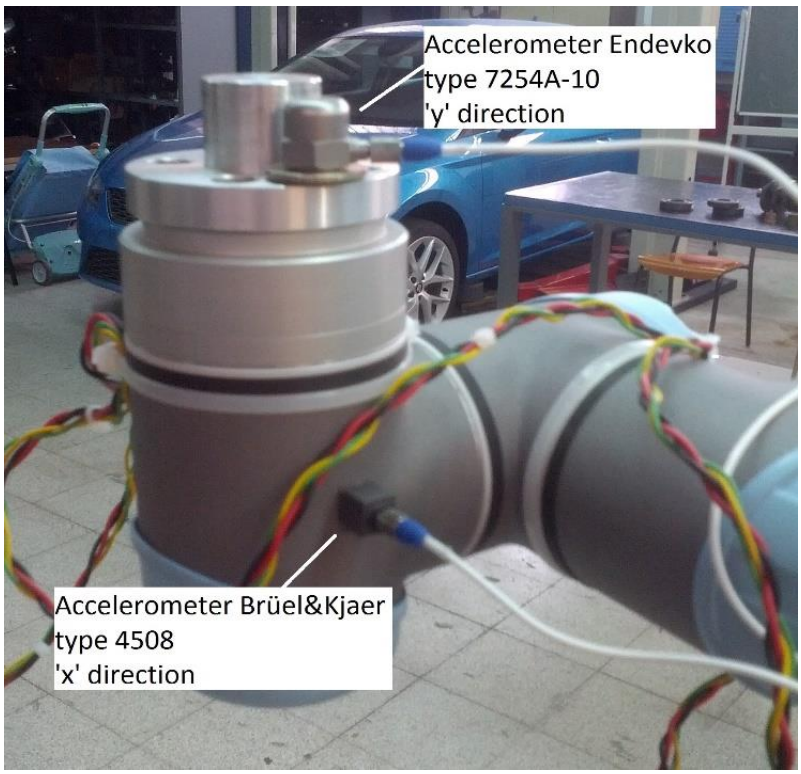


***Figure 2.4****: Detail of the end effector. On the top, the accelerometer Endevco type 7254 A-10 placed in vertical direction. On the bottom, the accelerometer Brüel & Kjær type 4508 placed in horizontal direction.*

Data acquisition system is Dewe-43 connected to an HP laptop via USB with software Dewesoft v.6.6.2.


***Figure 2.5**: data acquisition system Dewe-43 and Hp laptop.*

The acceleration signals for both channels are filtered and integrated to obtain the vibration velocity signals. The acceleration signals are affected by high frequency noises that can be reduced by applying a low pass filter, while the integration is required for obtaining velocities. The maximum frequency is supposed to be lower than $800$ Hz, thus the sampling rate is set to $2000$ Hz according to the Nyquist-Shannon theorem. The acquisition system automatically applies an anti-aliasing digital filters that eliminates the frequencies above $1000$ Hz.

## 2.3. Data elaboration

The software used for data analysis is DaDiSP Free Student Edition. This is a Digital Signal Processing software, which allows one to display and manipulate data series with an interface similar to a spreadsheet. DaDiSP worksheet consists of multiple interrelated windows where each window contains an entire series or a multi-column matrix.

Rough data from acquisition system Dewe-43 are saved as Text files in the HP laptop. These files are composed by the heading that specifies the details about the measurement acquisition, and three columns: Time, Vertical Velocity and Horizontal Velocity. The sample rate is 2000 Hz and the duration of the measurements is about 15 seconds, thus approximately thirty thousand samples are acquired for each measurement. This number is inferior to the maximum available for the Free Student Edition, 32678 points.

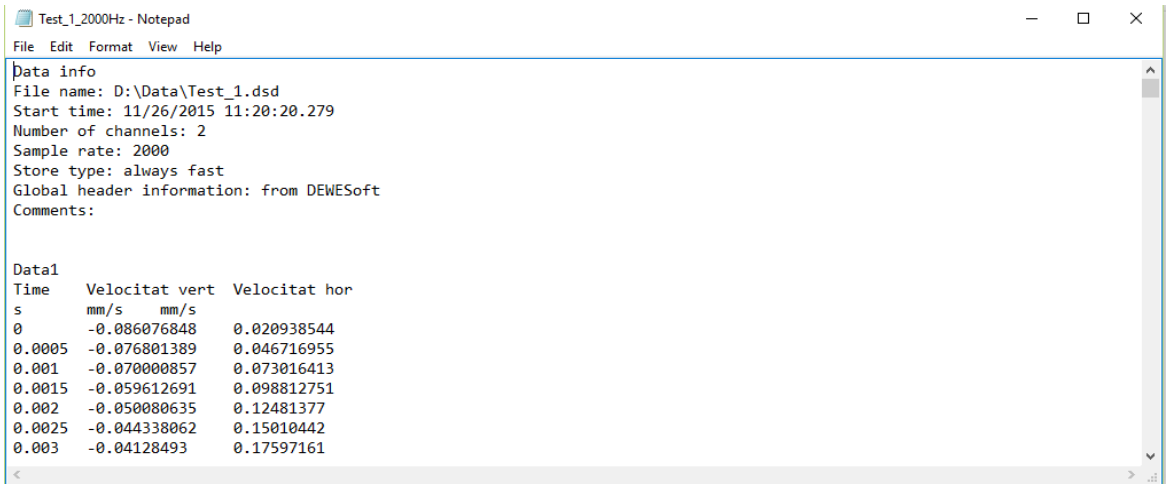


***Figure 2.6**: Data are acquired and saved in Text files. These are composed by heading and the three columns that are Time, Vertical Velocity and Horizontal Velocity.*

Text files are imported in DaDiSP software as ASCII files and placed in window W1.

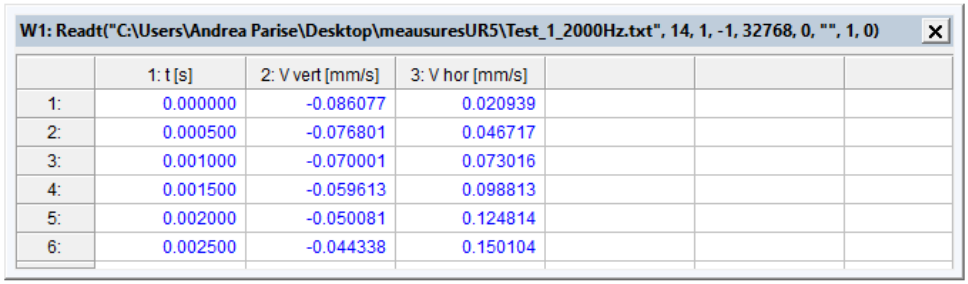


| | 1: t [s] | 2: V vert [mm/s] | 3: V hor [mm/s] |
|---|---|---|---|
| 1: | 0.000000 | -0.086077 | 0.020939 |
| 2: | 0.000500 | -0.076801 | 0.046717 |
| 3: | 0.001000 | -0.070001 | 0.073016 |
| 4: | 0.001500 | -0.059613 | 0.098813 |
| 5: | 0.002000 | -0.050081 | 0.124814 |
| 6: | 0.002500 | -0.044338 | 0.150104 |

***Figure 2.7**: Text files are imported as ASCII files and placed in the first window W1.*

Two velocity diagrams are generated composing the Time column and the Velocity column: window W3 represents Vertical Velocity and window W5 Horizontal Velocity.

Data may be displayed in several interactive forms including 2D graphs, XYZ plots and numeric tables. 2D graphs are the most convenient representation.

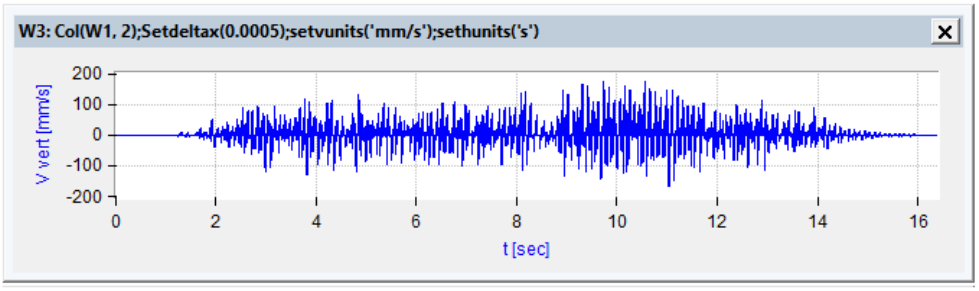


***Figure 2.8**: In window 3, the velocity diagram is generated by using Time column and Vertical Velocity column. The same operation is performed with Time column and Horizontal Velocity column in window 5.*

The command “Fast Fourier Transform FFT/spectral” is applied to generate the power frequency spectrum.

According to Parseval's theorem, the total mean power of the signal is:

$$\psi_x^2 = \frac{1}{T}\int_0^T x(t)^2 dt = \sum_{k=1}^{N} x_k^2$$

In which $x_k$ are the sampled values of velocity and $N$ is the total number of a measurement.

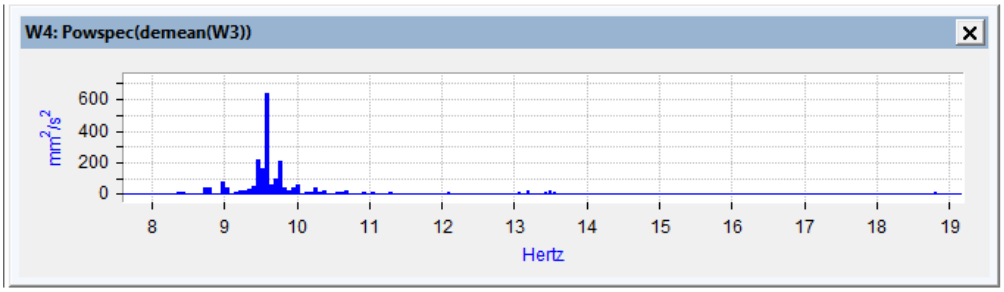


***Figure 2.9**: The frequency spectrum of the signal is obtained using the command FFT/spectrum. The main frequencies are shown.*

In Figure 2.10, the signal elaboration of the first acquisition is represented.

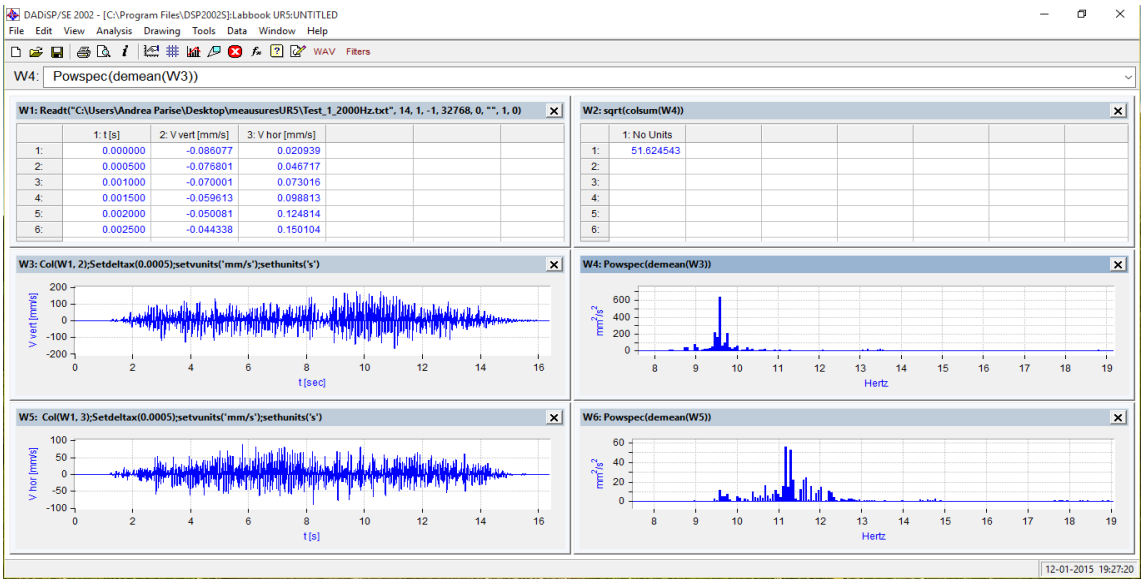


***Figure 2.10**: Complete interface with all the six windows for elaborating the data signal.*

The frequency corresponding to the maximum amplitude is the most significant. The Amplitude values however are very different during the tests: low repeatability depends on the impossibility to control the velocity of the platform during the tests because the platform is moved manually.

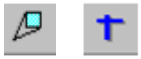

It is possible to determine the frequency corresponding to the maximum amplitude graphically by zooming the specific window.

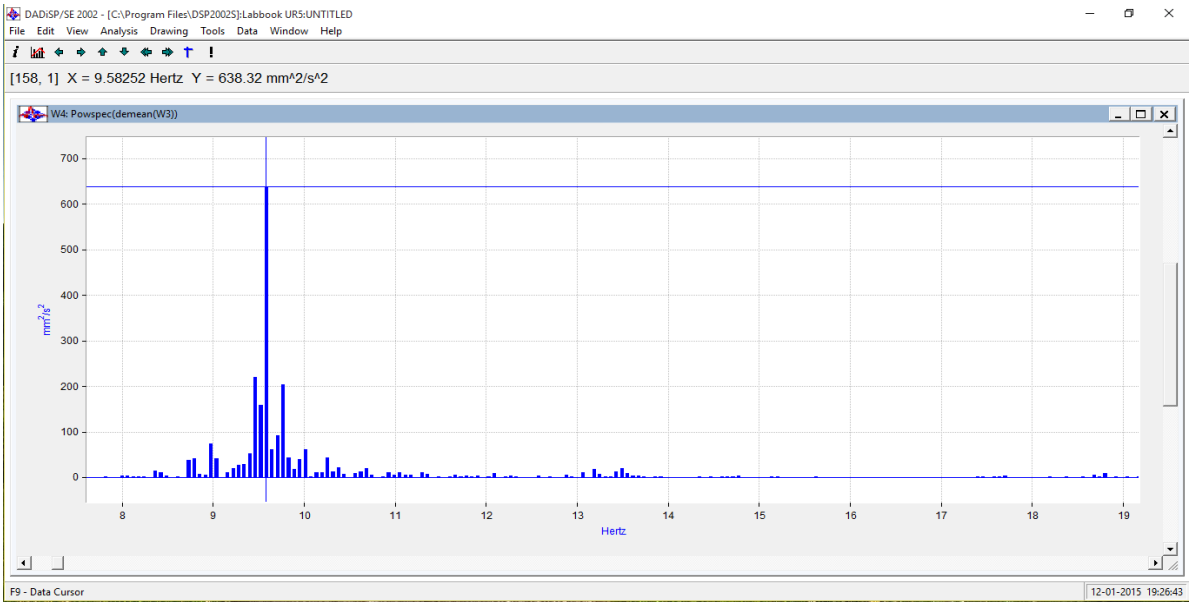


***Figure 2.11**: Particular detail of window W4. The frequency spectrum is zoomed and the coordinates of the main frequency are displayed using the data cursor button on the toolbar.*

The data elaboration allows to obtain the main frequencies for the Vertical Velocities $f_{V_v}$ and the Horizontal Velocity $f_{H_v}$, and their amplitude. The results are shown in Table 2.1.

| Test Nr | $f_{V_v}$ [Hz] | Amplitude $V_v$ $\left[\frac{mm^2}{s^2}\right]$ | $f_{H_v}$ [Hz] | Amplitude $H_v$ $\left[\frac{mm^2}{s^2}\right]$ | Push/ /Pull | Horizontal/ /Forward | Power on/ /Power off |
|---|---|---|---|---|---|---|---|
| **1st** | 9,58 | 638 | 11,17 | 56,1 | Push | Horizontal | Off |
| **2nd** | 9,03 | 245 | 11,17 | 36,2 | Pull | Horizontal | Off |
| **3rd** | 9,58 | 305 | 11,17 | 33,3 | Push | Horizontal | Off |
| **4th** | 9,09 | 11,75 | 11,66 | 12,28 | Push | Horizontal | On |
| **5th** | 8,79 | 20,6 | 10,90 | 15,3 | Pull | Horizontal | On |
| **6th** | 10,31 | 11,56 | 11,35 | 12,07 | Push | Horizontal | On |
| **7th** | 14,80 | 19,2 | 14,40 | 9,04 | Pull | Forward | On |
| **8th** | 14,65 | 16,46 | 14,04 | 7,55 | Push | Forward | On |
| **9th** | 14,47 | 51,75 | 14,10 | 12,6 | Pull | Forward | Off |
| **10th** | 14,78 | 57 | 14,77 | 16,59 | Push | Forward | Off |

***Table 2.1****: This table reports the results and details of the ten tests. These were accomplished pushing and pulling the mobile platform with conventional wheels in two different arms configurations with joints powered or braked.*

Two cases, in which the frequency behaviour is similar, are identified:

| Case | Position | N° measurement |
|---|---|---|
| **1** | Horizontal | 1, 2, 3, 4, 5, 6 |
| **2** | Forward | 7, 8, 9, 10 |

***Table 2.2****: Index of the two cases.*

The influence of motion generation, i.e. push/pull, is negligible and does not affect the values of measurements. Another observation is that the state of the joints is also negligible. The behaviour of the mobile robot is approximately the same when powered or braked. This may help in the future implementation of the analytical model in which the joints' stiffness is considered.

The average frequencies of Vertical and Horizontal Velocities and the corresponding cut-off frequencies are calculated:

| Case | Position | $f_{Vv}$ [Hz] | $f_{Hv}$ [Hz] |
|---|---|---|---|
| **1** | Horizontal | 9,40 | 11,24 |
| **2** | Forward | 14,68 | 14,33 |

***Table 2.3**: Frequencies calculation.*

With both arms extended in horizontal position, the differences between joint motors powered and braked are very small: the average value of the frequencies referred to Vertical Velocity is $9{,}40$ Hz and the one referred to Horizontal Velocity is $11{,}24$ Hz.

With both arms folded in forward configuration, the system is more compact and the inertia moment is lower, thus natural frequencies are higher than in the horizontal position, in particular, the averages are $14{,}68$ Hz for the Vertical Velocity and $14{,}33$ Hz for the Horizontal Velocity.

It is possible to consider the Vertical Velocity and its frequency $f_{Vv}$ related to the first degree of freedom, the translation along z-axis expressed by the variable '***z***'. The Horizontal Velocity and its frequency $f_{Hv}$ are related to the second degree of freedom, the rotation around the y-axis expressed by the variable *'$\vartheta$'*, according to the reference system introduced in Figure 2.1 at the beginning of the chapter.

Low frequencies generate the most critical vibrations because they are closer to the resonance frequency, which is the natural frequency of the system. On one hand, it is necessary to lower as possible the resonance frequency of the mobile robot in order to have good attenuation of the vibrations. On the other hand, it is possible to reduce the generation itself using the mobile robot on smooth floors without flaws and defects, in an isolated and controlled environment.

# 3. Vibration isolation

The problem of vibration isolation is presented in two different ways.

Mechanical systems generate inertia forces while they are operating and those are transmitted to the pavement. With the use of elastic isolators, active vibration isolation is realized to limit the amplitude of the transmitted forces to the base.

Mechanical systems are affected by external vibrations transmitted by the pavement. Using elastic isolators, passive vibration isolation is realized to limit the amplitude of the vibrations transmitted to the mechanical systems.

In this chapter, passive vibration isolation is explained and analysed.

## 3.2. Passive vibration isolation

To introduce a vibration isolation problem, a one degree of freedom system, composed by mass $M$, spring $k$ and damper $c$, is considered. It is affected by an external harmonic vibration $s(t) = s_0 \sin(\omega t)$ acting on the pavement to which the mass is linked by spring and damper.

In order to study the behaviour of the system, the Transmissibility is the parameter that describes the response of the mass afflicted by the external disturbance.

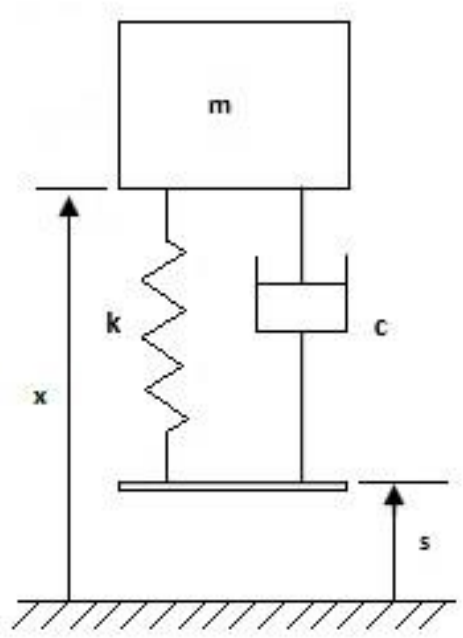


***Figure 3.1**: Mass-spring-damper system in a passive vibration isolation example.*

Vertical displacement of the pavement provokes the transmission of the elastic force $F_k$ and the damping force $F_c$ to the mass $m$.

The equation of the motion is:

$$m\ddot{x} = F_k + F_c$$

With:

$F_k = -k(x - s)$

$F_c = -c(\dot{x} - \dot{s})$

$$m\ddot{x} = -k(x - s) - c(\dot{x} - \dot{s}) \quad \rightarrow \qquad m\ddot{x} + c\dot{x} + kx = c\dot{s} + ks$$

The motions of the mass $x$ and the base $s$ are expressed in complex formulation:

$$s = s_0 e^{j\omega t}$$

$$x = x_0 e^{j\omega t}$$

With $s_0$ and $x_0$ the amplitudes.

It becomes:

$$-m\omega^2 x_0 e^{j\omega t} + jc\omega x_0 e^{j\omega t} + kx_0 e^{j\omega t} = jc\omega s_0 e^{j\omega t} + kx_0 e^{j\omega t}$$

$$[(k - m\omega^2) + jc\omega]x_0 = (k + jc\omega)s_0$$

$$\frac{x_0}{s_0} = \frac{k + jc\omega}{(k - m\omega^2) + jc\omega}$$

The Transmissibility is:

$$T = \frac{|x_0|}{|s_0|} = \sqrt{\frac{{x_0}^2}{{s_0}^2}} = \frac{\sqrt{k^2 + c^2\omega^2}}{\sqrt{(k - m\omega^2)^2 + c^2\omega^2}}$$

Defining $\omega_n$ as the natural pulsation and $\xi$ as the damping ratio:

$${\omega_n}^2 = \frac{k}{m} \qquad \xi = \frac{c}{2\sqrt{k\,m}}$$

The numerator becomes:

- $(k^2 + c^2\omega^2) = k^2\left(1 + \frac{c^2\omega^2}{k^2}\right) = k^2\left(1 + 4\frac{c^2}{4\,km}\cdot\frac{m\,\omega^2}{k}\right) = k^2\left(1 + \left(2\xi\frac{\omega}{\omega_n}\right)^2\right)$

The denominator becomes:

- $(k - m\omega^2)^2 = k^2\left(1 - \frac{m\,\omega^2}{k}\right)^2 = k^2\left(1 - \frac{\omega^2}{{\omega_n}^2}\right)^2$
- $c^2\omega^2 = k^2\left(4\frac{c^2}{4\,km}\cdot\frac{m\,\omega^2}{k}\right) = k^2\left(2\xi\frac{\omega}{\omega_n}\right)^2$

The Transmissibility is:

$$T = \frac{|x_0|}{|s_0|} = \frac{\sqrt{1 + \left(2\xi \frac{\omega}{\omega_n}\right)^2}}{\sqrt{\left(1 - \frac{\omega^2}{{\omega_n}^2}\right)^2 + \left(2\xi \frac{\omega}{\omega_n}\right)^2}}$$

The Phase angle is:

$$\varphi_0 = -arctan\frac{c\omega\, x_0}{(k - m\omega^2)\, x_0} + arctan\frac{c\omega\, s_0}{k\, s_0} = -arctan\frac{2\xi \frac{\omega}{\omega_n}}{1 - \frac{\omega^2}{{\omega_n}^2}} + arctan 2\xi \frac{\omega}{\omega_n}$$

The graphic representation of the Transmissibility is:

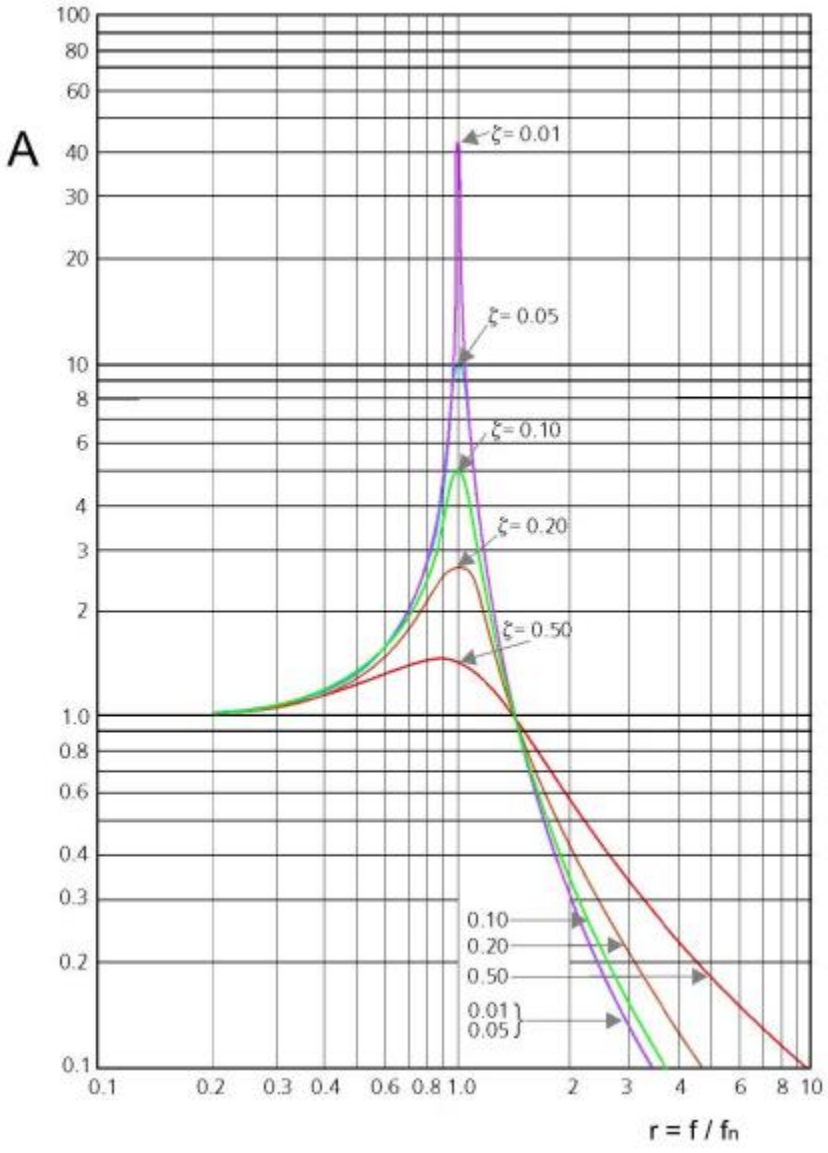


***Figure 3.2**: Graphic representation of the Transmissibility depending on the value of damping.*

Figure 3.2 represents the Transmissibility. Three regions with different behaviours of the system are distinguished, namely:

1) For $0 \leq {}^{\omega}/_{\omega_n} < 0{,}2$ the transmission of the motion is approximately rigid. T>1.

2) For $0{,}2 \leq {}^{\omega}/_{\omega_n} < \sqrt{2}$ the vibration amplitude of the system mass is amplified. The lower the values of damping, the higher the peak of amplitude. T>1.

3) For ${}^{\omega}/_{\omega_n} \geq \sqrt{2}$ the vibration amplitude of the system mass is reduced. The lower the values of the damping ξ, the higher the reduction of amplitude. This region represents the most significant part for isolating systems. T<1.

The Attenuation Factor (A.F.) is another parameter expressed in percentage that describes the output reduction of the vibration:

$$A.F. = 1 - T \ \ (\%)$$

High values of damping help containing amplification in resonance region but attenuate the isolation for $\omega > \sqrt{2}\omega_n$. A low value of damping is required to achieve good isolation: a typical value for commercial products is approximately $\xi = 0{,}1$.

As previously mentioned, the mobile robot has to move on the plant and has to overcome obstacles. Impulsive bumps generate a wide vibration spectrum characterized by very low frequencies up to 20-30 Hz. The main aim is to attenuate as much as possible the vibration levels in the platform, by reducing the transmissibility from base to platform, and to avoid propagation from platform to manipulators. The choice of the springs is therefore very important. They are characterized by soft stiffness and high vertical deflection in order to reduce the value of the natural frequency. In this way, the graph of the Transmissibility would be shifted to low frequencies, increasing the extension of region 3 and reducing regions 1 and 2.

The number and location of the springs used are fundamental to evaluate the global stiffness and the stability of the platform. Changes of direction or value of the velocity of the platform generate inertia forces acting on the gravity centre. Its position is distant from the platform more than $500\ \mathrm{mm}$, thus the deflections of the isolation system due to inertia moment represent a stability problem.

# 4. Design of the isolation system

The following chapter of the thesis is about the theoretical model and the choice of the stiffness of the isolation system from catalogue. Two different technologies are presented and the differences between them are analysed.

## 4.1 Theoretical model

The isolator system is composed by four elements arranged in square. The damping is supposed to be negligible for the sake of model simplicity: its value is usually very small in order to have more vibration isolation, as previously shown. Three is the minimum number of isolators that is possible to introduce on the platform, but four is more functional. With four isolators, the stability of the mobile robot is enhanced: the dimensions of the isolators are little, hence the problems of space, discussed for motor groups, are not relevant. Figure 4.1 displays the disposition of the isolator system and motor groups on the platform.

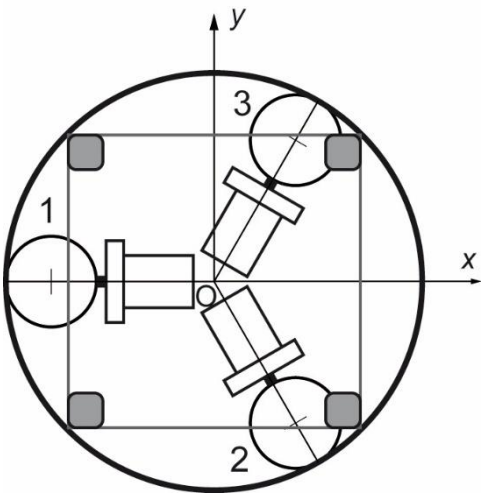


***Figure 4.1****: Disposition of isolation system and motor groups on the platform* [1]*.*

A model with two degrees of freedom is implemented to study the vibrational behaviour of the mobile robot. It describes the vertical displacement $z$ along the z-axis and the pitch rotation $\vartheta$ of the platform around the y-axis.

The symmetrical geometry of the platform and the square arrangement of the isolation system allow to use a simple theoretical model. The translational motions along the x-axis and the y-axis generate the same dynamic equations, thus the model can be simplified.

In Figure 4.2, the representation of the model is given.

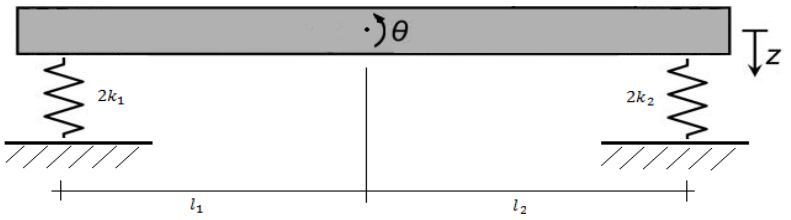


***Figure 4.2**: Representation of the model with two degrees of freedom.*

The equations that describe the motion are:

$$\begin{cases} m\,\ddot{z} + 2k_1(z + l_1\vartheta) + 2k_2(z - l_2\vartheta) = 0 \\ I_y^G\ddot{\vartheta} + 2k_1l_1(z + l_1\vartheta) + 2k_2l_2(z - l_2\vartheta) = 0 \end{cases}$$

With:

$l_1 = l_2 = l = 235\ \text{mm}$,

$m = 128{,}8\text{kg}$,

$I_{yy} = 37{,}8\text{kgm}^2$,

$k_1, k_2$ to be determined.

In matrix representation:

$$\begin{bmatrix} m & 0 \\ 0 & I_y^G \end{bmatrix}\begin{pmatrix} \ddot{z} \\ \ddot{\vartheta} \end{pmatrix} + \begin{bmatrix} 2k_1 + 2k_2 & 2k_1\text{l} - 2k_2l \\ 2k_1l - 2k_2l & 2k_1l^2 + 2k_2l^2 \end{bmatrix}\begin{pmatrix} z \\ \vartheta \end{pmatrix} = \begin{pmatrix} 0 \\ 0 \end{pmatrix}$$

It is possible to uncouple the two degrees of freedom if the non-diagonal terms of the stiffness matrix are zero. The practical explanation is that vertical vibrations do not activate pitch vibration, and vice versa. The decoupling reduces the system from two degrees of freedom to two basic systems with one degree of freedom. In this way, the equations of the motion are simpler and the behaviour of the whole system is easier to control. The relation between the values of stiffness of the isolators is:

$$2k_1l - 2k_2l = 0 \qquad \rightarrow \qquad k_1 = k_2 = k$$

In matrix representation it is:

$$\begin{bmatrix} m & 0 \\ 0 & I_y^G \end{bmatrix}\begin{pmatrix} \ddot{z} \\ \ddot{\vartheta} \end{pmatrix} + \begin{bmatrix} 4k & 0 \\ 0 & 4kl^2 \end{bmatrix}\begin{pmatrix} z \\ \vartheta \end{pmatrix} = \begin{pmatrix} 0 \\ 0 \end{pmatrix}$$

Assuming the variables in the following formulation:

$$z = z_0 \sin(\omega_n t) \qquad \dot{z} = \omega_n z_0 \cos(\omega_n t) \qquad \ddot{z} = -\omega_n^2 z_0 \sin(\omega_n t)$$
$$\vartheta = \vartheta_0 \sin(\omega_n t) \qquad \dot{\vartheta} = \omega_n \vartheta_0 \cos(\omega_n t) \qquad \ddot{\vartheta} = -\omega_n^2 \vartheta_0 \sin(\omega_n t)$$

$$-\omega_n^2 \begin{bmatrix} m & 0 \\ 0 & I_y^G \end{bmatrix} \begin{pmatrix} z_0 \\ \vartheta_0 \end{pmatrix} \sin \omega_n t + \begin{bmatrix} 4k & 0 \\ 0 & 4kl^2 \end{bmatrix} \begin{pmatrix} z_0 \\ \vartheta_0 \end{pmatrix} \sin \omega_n t = \begin{pmatrix} 0 \\ 0 \end{pmatrix}$$

$$\begin{bmatrix} 4k - \omega_n^2 \, m & 0 \\ 0 & 4kl^2 - \omega_n^2 I_y^G \end{bmatrix} \begin{pmatrix} z_0 \\ \vartheta_0 \end{pmatrix} = \begin{pmatrix} 0 \\ 0 \end{pmatrix}$$

Natural pulsations are the solutions of the characteristic equation obtained by cancelling the determinant of the matrix:

$$(4k - \omega_n^2 \, m) \cdot \left(4kl^2 - \omega_n^2 I_{yy}\right) = 0$$

The two natural frequencies and the corresponding cut-off frequencies are:

$$\omega_{n1} = \sqrt{\frac{4\,k}{m}} \quad \rightarrow \quad f_{n1} = \frac{1}{2\pi}\omega_{n1} = \frac{1}{2\pi}\sqrt{\frac{4\,k}{m}} \quad \rightarrow \quad f_{c1} = \sqrt{2} f_{n1}$$

$$\omega_{n2} = \sqrt{\frac{4\,k\,l^2}{I_y^G}} \quad \rightarrow \quad f_{n2} = \frac{1}{2\pi}\omega_{n2} = \frac{1}{2\pi}\sqrt{\frac{4\,k\,l^2}{I_y^G}} \quad \rightarrow \quad f_{c2} = \sqrt{2} f_{n2}$$

## 4.2. Choice of springs

The isolation system, as previously shown, is composed by four elements arranged in square and its purpose is to realize passive vibration isolation.

The disturbance, which the mobile robot is subjected to, is not characterized by one particular frequency, rather by a wide low frequency spectrum from $5$ to $20\,\mathrm{Hz}$, caused by impulsive solicitations that may happen during the motion of the platform.

The cut-off frequencies of the mobile robot should be lower than the wide spectrum of frequencies in order to have a good attenuation, thus the stiffness of the system has to be low and this requires the use of very soft springs.

Dimension is another important aspect to consider: the elements have to be small and compact. Therefore, the choice of the type of isolator is a delicate decision.

Common passive isolation systems adopted for completing this task are composed principally by pneumatic or air isolators, or mechanical wire rope isolators.

***Figure 4.3a**: Wire rope isolators.*

***Figure 4.3b**: Pneumatic isolators* [6].

There are several differences between these two categories.

Considering two elements with the same stiffness, wire rope isolators require larger space and huger deflections to provide soft stiffness. Pneumatic isolators, instead, are characterized by contained deflections and dimensions, thus they can be placed easily on the platform near motor groups. Furthermore, supplied with a tank valve, pneumatic isolators can be inflated and levelled manually using a hand pump or air chuck connected to an air supply. In this way, it is possible to regulate pressure and height of few millimetres in order to keep the system in plane.

The costs of rope isolators and pneumatic isolators are approximately the same.

Both these elements have little internal damping, that provides good isolation and helps extinguishing the vibrational phenomenon, but their natures are different. Wire rope isolators have hysteretic damping while pneumatic isolators viscous damping. Hysteretic damping, typical of metallic materials, is described by a force proportional to the displacement but in phase with the

velocity, instead viscous damping, typical of fluids, is described by a force proportional to the velocity. The period of oscillation is different: with viscous damping the period is $= \frac{2\pi}{\omega_n\sqrt{1-\xi^2}}$ , while with hysteretic damping is $T = \frac{2\pi}{\omega_n}$. Since the value of damping is little, the difference in the periods of oscillation is negligible.

For these reasons Pneumatic isolators are preferred to wire rope isolators.

Different catalogues are examined to find the optimal solution.

The pneumatic isolators introduced on the platform are four and the type is:

“Precision-Aire™ - Pneumatic Leveling Mounts PLM1” from Fabreeka [6]:

PLM Mount Specifications

| Model | Dimensions | | | | | | | | | Max Load |
|---|---|---|---|---|---|---|---|---|---|---|
| | A | B | C | D* | E | F | G | H | I | |
| PLM 1 | 3.00 in<br>76 mm | 2.38 in<br>60.5 mm | 0.28 in<br>6.9 mm | 0.375-16<br>M10 | 0.47 in<br>12.0 mm | 2.88 in<br>73 mm | 1.00 in<br>25 mm | 2.50 in<br>65 mm | 0.125 in<br>3.2 mm | 100 lbs<br>45 Kg |

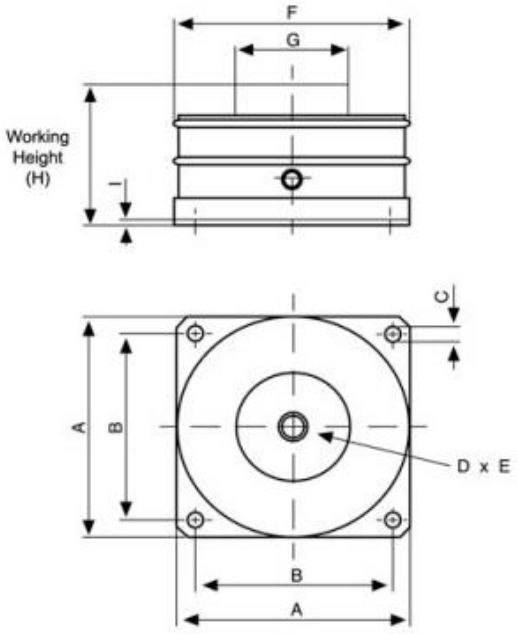


***Figure 4.4**: Representation of the PLM1 pneumatic isolator* [6].

Characteristics:

Maximum Force: $F_{max} = 441{,}5\ \mathrm{N}$

Working Height: $H = 65\ \mathrm{mm}$

Stiffness: $k = \frac{F_{max}}{H} = \frac{441{,}5}{65} = 6{,}8\ ^{\mathrm{N}}/_{\mathrm{mm}}$

The natural frequencies and cut-off frequencies of the system are:

$$f_{n1} = \frac{1}{2\pi}\sqrt{\frac{4k}{m}} = \frac{1}{2\pi}\sqrt{\frac{4 \cdot 6800}{128{,}8}} = 2{,}3 \text{ Hz} \qquad f_{c1} = \sqrt{2} f_{n1} = 3{,}3 \text{ Hz}$$

$$f_{n2} = \frac{1}{2\pi}\sqrt{\frac{4kl^2}{I_y^G}} = \frac{1}{2\pi}\sqrt{\frac{4 \cdot 6800 \cdot 0{,}235^2}{37{,}8}} = 1{,}0 \text{ Hz} \qquad f_{c2} = \sqrt{2} f_{n2} = 1{,}4 \text{ Hz}$$

The introduction of the isolation system on one hand enhances the accuracy of the mobile robot, but on the other hand introduces problems connected to the stability. When the manipulators are operating or the platform is moving, in particular during the acceleration and deceleration phases, inertia forces provoke the generation of a transient oscillation, characterised by low frequency. The response of the mobile robot to different types of acceleration inputs is analysed in the following chapter.

The output reduction of the vibrations and the efficiency of the isolation system are estimated by considering the Transmissibility for the two degrees of freedom system:

$$T = \frac{\sqrt{1 + \left(2\xi \frac{\omega}{\omega_n}\right)^2}}{\sqrt{\left(1 - \frac{\omega}{\omega_n}^2\right)^2 + \left(2\xi \frac{\omega}{\omega_n}\right)^2}}$$

With $\xi = 0{,}1$.

According to the reference system introduced in Figure 2.1, the frequency $f_{Vv}$ is related to the first degree of freedom, the translation along the z-axis expressed by the variable '***z***', while the frequency $f_{Hv}$ is related to the second degree of freedom, the rotation around the y-axis expressed by the variable *'$\vartheta$'*.

Mobile robot's main frequencies without the isolation system are obtained with the extended manipulators set in the horizontal configuration, while mobile robot's main frequencies with the isolation system have been previously evaluated.

Without isolation system: $f_1 = 9{,}4\text{Hz}$ and $f_2 = 11{,}2\text{Hz}$.
With isolation system: $f_{n1} = 2{,}3\text{Hz}$ and $f_{n2} = 1{,}0\text{Hz}$.

- For the first degree of freedom the Transmissibility is:

$$T_1 = \frac{\sqrt{1 + \left(2 \cdot 0{,}1 \cdot \frac{9{,}4}{2{,}3}\right)^2}}{\sqrt{\left(1 - \frac{9{,}4^2}{2{,}3^2}\right)^2 + \left(2 \cdot 0{,}1 \cdot \frac{9{,}4}{2{,}3}\right)^2}} = 0{,}083 = 8{,}3\%$$

The Attenuation Factor is 91,7%.

- For the second degree of freedom:

$$T_2 = \frac{\sqrt{1 + \left(2 \cdot 0{,}1 \cdot \frac{11{,}2}{1{,}0}\right)^2}}{\sqrt{\left(1 - \frac{11{,}2^2}{1{,}0^2}\right)^2 + \left(2 \cdot 0{,}1 \cdot \frac{11{,}2}{1{,}0}\right)^2}} = 0{,}048 = 4{,}8\%$$

The Attenuation Factor is 95,2%.

# 5. Response during the transient motion

The main peculiarity of a mobile robot is the possibility of moving and completing complex manipulations in the most flexible way. Transient actions, as the motion of platform and the activities of manipulators, generate inertia forces that negatively influence the stability and accuracy of the system. Commons problems are the loss of the grip of the object and the accidental collisions with the environment that may invalidate the performance of the operation. The attention is focused principally on the effects of profile of acceleration assigned to the platform. In particular, the acceleration profile is the parameter that conditions most the behaviour of the mobile robot.

In this chapter, the system's responses to different acceleration inputs are evaluated and their differences are analysed.

## 5.1. Response to step input of acceleration

The law of the motion assigned to the system is an acceleration step input as shown in Figure 5.2.

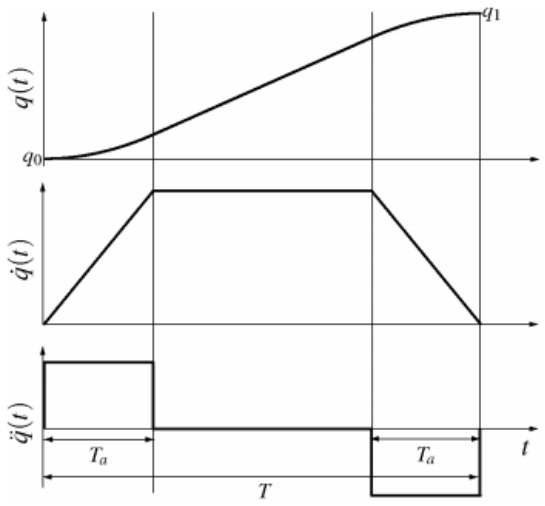


***Figure 5.1**: Law of the motion: acceleration step input.*

Joints of manipulators for assembling tasks usually operate following a step input acceleration law of motion, this happens because it takes less time to complete the same operation compared to other laws of motion. The cycle time is one of the most important parameters to minimize in order to make repetitive tasks economically competitive, however this does not mean that focusing only on that aspect is always the best choice.

For example, let $q(t)$ be the angle variation that a rotational joint has to describe in two different times span $T_2 = \alpha \cdot T_1$ with $\alpha > 1$. Deriving $q(t)$:

$$q_1(t) = q_2(\alpha \cdot t) \qquad \rightarrow \qquad \dot{q_1}(t) = \alpha \cdot \dot{q_2}(\alpha \cdot t) \qquad \rightarrow \qquad \ddot{q_1}(t) = \alpha^2 \cdot \ddot{q_2}(\alpha \cdot t)$$

The shorter the time span, the higher the values of velocity and acceleration. The maximum values are increased respectively by $\alpha$ and $\alpha^2$, thus the reduction of the cycle time causes the increase of inertia effects proportional to the square of the factor $\alpha$.
The model considers only the rotational degree of freedom, assuming that the isolation system works only in the vertical direction. Horizontal displacements are negligible, for the sake of model simplicity.

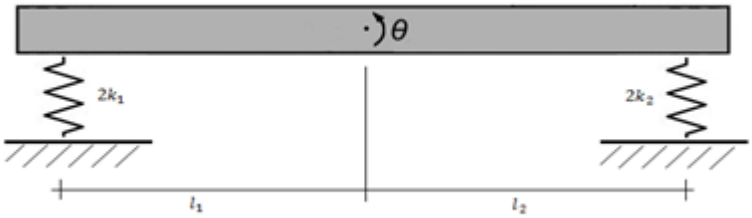


***Figure 5.2**: Representation of the model.*

The value of acceleration imposed by technical specifications is $a_y = 1\,{}^{\mathrm{m}}/_{\mathrm{s}^2}$, thus the inertia force applied to the gravity centre is:

$$F_i = m \cdot a_y = 128{,}8 \cdot 1 = 128{,}8\ \mathrm{N}$$

The momentum applied to the rotation point O is:

$$M_i = F_i \cdot h = 128{,}8 \cdot 0{,}524 = 67{,}5\ \mathrm{Nm}$$

The input of acceleration $\ddot{\vartheta}_{in}$ is:

$$\ddot{\vartheta}_{in} = \frac{M_i}{I_x^O} = \frac{67{,}5}{77{,}5} = 0{,}87\ \frac{\mathrm{rad}}{\mathrm{s}^2}$$

### 5.1.1. Step input without damping

The study is developed only for the first step of the profile of acceleration. Similar conclusions can be drawn for the other parts of the law of motion. The case without damping represents the worst case scenario in terms of overshoot, because the maximum values of acceleration is twice the value of the step input.

The correspondent dynamic equation without damping is:

$$I_x^O \ddot{\vartheta} + 2k(l_1^2 + l_2^2)\,\vartheta = F_i\, h\, g_i \qquad \rightarrow \qquad I_x^O \ddot{\vartheta} + 4kl^2\,\vartheta = F_i\, h\, g_i$$

With $= 6800\ {}^{\mathrm{N}}/_{\mathrm{m}}$ , $l_1 = l_2 = l = 0{,}235\ \mathrm{mm}$ and $g_i$ the unitary input.

Using the Laplace Transform, one gets:

$$I_x^O s^2\,\Theta(s) + 4kl^2\,\Theta(s) = F_i\, h \cdot \frac{1}{s}$$

$$\frac{I_x^O}{4kl^2} s^2\,\Theta(s) + \Theta(s) = \frac{F_i\, h}{4kl^2} \cdot \frac{1}{s}$$

With:

$4kl^2 = k_{eq}$.

$$\frac{I_x^O}{k_{eq}} s^2 \Theta(s) + \Theta(s) = \frac{1}{s} \cdot \Theta_{in}$$

Introducing the representation:

$\frac{I_x^O}{k_{eq}} = \frac{1}{{\omega_n}^2}$

With $\xi = 0{,}1$ and $\omega_n = 4{,}4\ {}^{\mathrm{rad}}/_{\mathrm{s}}$.

The expression becomes:

$$\left(1 + \frac{1}{{\omega_n}^2} s^2\right) \cdot \Theta(s) = \frac{1}{s} \cdot \Theta_{in}$$

The Transfer Function *T.F.* is:

$$T.F. = \frac{\Theta(s)}{\Theta_{in}} = \frac{1}{1 + \frac{1}{{\omega_n}^2} s^2} \cdot \frac{1}{s} = \frac{{\omega_n}^2}{s^2 + {\omega_n}^2} \cdot \frac{1}{s}$$

By evaluating the inverse Laplace transform:

$$\vartheta(t) = \vartheta_{in}(1 - \cos 2\pi f_n t)$$

The maximum overshoot is:

$$|\vartheta_{max}| = \vartheta_{in}|1 - \cos \omega_n t| \leq 2\,\vartheta_{in}$$

The graphic response to a step input acceleration without damping is:

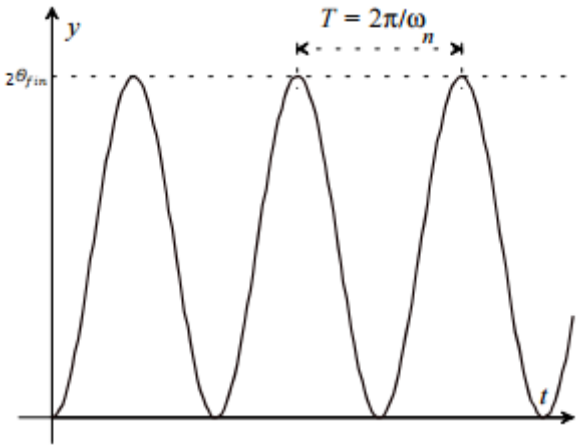


***Figure 5.3**: Response of the system to a step input of acceleration. Overshoot is twice the value of the input*

### 5.1.2. Step input for the system with damping

The presence of small damping allows to reduce the maximum overshoot that affects the mobile robot, and settles the vibrations. The corresponding equation with damping is:

$$I_x^O \ddot{\vartheta} + 2c(l_1^2 + l_2^2)\dot{\vartheta} + 2k(l_1^2 + l_2^2)\,\vartheta = F_i\, h\, g_i$$

With:

$l_1 = l_2 = l = 0{,}235\ \text{mm}$,

$F_i$ is the inertia force,

Using the Laplace Transform:

$$I_x^O s^2\,\Theta(s) + 4cl^2 s\,\Theta(s) + 4kl^2\,\Theta(s) = F_i\, h \cdot \frac{1}{s}$$

$$\frac{I_x^O}{4kl^2} s^2\,\Theta(s) + \frac{4cl^2}{4kl^2} s\,\Theta(s) + \Theta(s) = \frac{F_i\, h}{4kl^2} \cdot \frac{1}{s}$$

$$\frac{I_x^O}{k_{eq}} s^2 \Theta(s) + \frac{c_{eq}}{k_{eq}} s\Theta(s) + \Theta(s) = \frac{1}{s} \cdot \Theta_{in}$$

The expression becomes:

$$\left(\frac{1}{{\omega_n}^2} s^2 + 2\frac{\xi}{\omega_n} s + 1\right) \cdot \Theta(s) = \frac{1}{s} \cdot \Theta_{in}$$

Where the Transfer Function *T.F.* is:

$$T.F. = \frac{\Theta(s)}{\Theta_{in}} = \frac{1}{\frac{s^2}{{\omega_n}^2} + 2\xi\frac{s}{\omega_n} + 1} \cdot \frac{1}{s} = \frac{{\omega_n}^2}{s^2 + 2\xi\omega_n s + {\omega_n}^2} \cdot \frac{1}{s}$$

The denominator has zeros:

$$s_{1,2} = \frac{-2\xi\omega_n \pm \sqrt{(2\xi\omega_n)^2 - 4{\omega_n}^2}}{2} = -\omega_n\left(\xi \pm i\sqrt{1-\xi^2}\right)$$

*T.F.* becomes:

$$T.F. = \frac{{\omega_n}^2}{\left[s + \omega_n\left(\xi + i\sqrt{1-\xi^2}\right)\right] \cdot \left[s + \omega_n\left(\xi - i\sqrt{1-\xi^2}\right)\right]} \cdot \frac{1}{s}$$

By evaluating the inverse Laplace transform:

$$\ddot{\vartheta}(t) = \ddot{\vartheta}_{in}\left[1 - \frac{e^{-\xi\omega_n t}}{\sqrt{1-\xi^2}}\sin\left(\omega_n t\sqrt{1-\xi^2} + \psi\right)\right]$$

With:

$$\psi = \cos^{-1}(\xi)$$

The graphic response to a step input acceleration of the system with damping is:

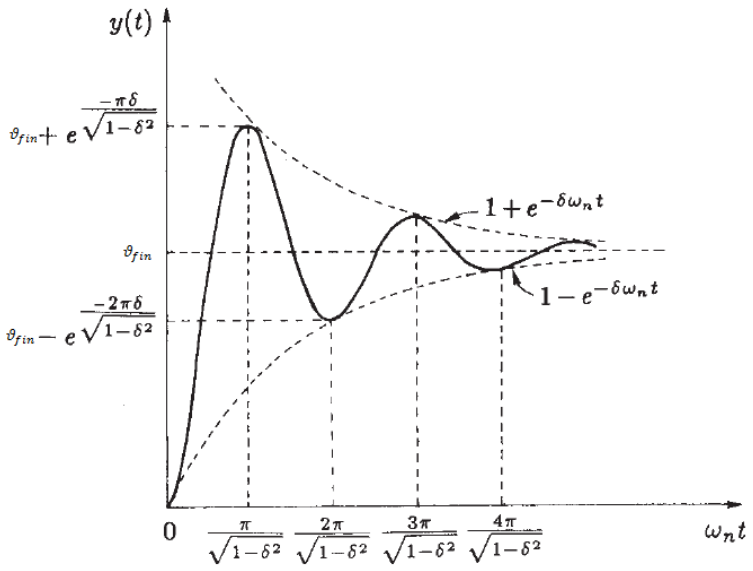


***Figure 5.4****: Graphic representation of the response of the damped system to a step input of acceleration. The response is confined between the two exponentials.*

The maximum overshoot is $\ddot{\vartheta}_{max} = \ddot{\vartheta}\left({}^{T}/_{2}\right)$ and the minimum $\ddot{\vartheta}_{min} = \ddot{\vartheta}(T)$:

$$\ddot{\vartheta}_{max} = \ddot{\vartheta}_{in}\left[1 - e^{\frac{-\xi\pi}{\sqrt{1-\xi^2}}} \cdot \frac{1}{\sqrt{1-\xi^2}}\sin(\pi + \psi)\right] = 1.73\ \ddot{\vartheta}_{fin}$$

$$\ddot{\vartheta}_{min} = \ddot{\vartheta}_{in}\left[1 - e^{\frac{-\xi 2\pi}{\sqrt{1-\xi^2}}} \cdot \frac{1}{\sqrt{1-\xi^2}}\sin(2\pi + \psi)\right] = 0.47\ \ddot{\vartheta}_{fin}$$

These results correspond to the extreme situation in which the acceleration value is maximum and the law of the motion is step input. The mobile robot does not use its full potentiality for the motion and the acceleration profile to use for the motion is not the step input, thus the displacements will not be so hard.

## 5.2. Response to a linear ramp acceleration input

The displacements of the mobile robot during the transient motion represent a problem for the stability. It is possible to limit the maximum overshoot by substituting the step input of acceleration with a linear ramp. This modification tries to reduce the discontinuity presented in the profile of acceleration that is the main cause of the instability.

The law of the motion is displayed in the Figure 5.6. The linear acceleration and the constant acceleration are considered for the analytical study of the response of the mobile robot.

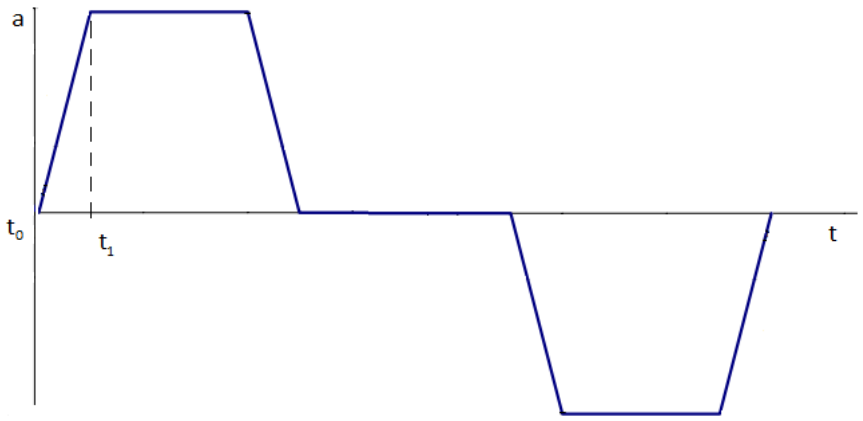


***Figure 5.5**: law of the motion with linear ramp input acceleration.*

The theoretical model is developed by neglecting the damping in order to overestimate the overshoot:

$$I_{xx}^{O}\ddot{\vartheta} + 2k(l_1^2 + l_2^2)\,\vartheta = M_i \cdot g_i$$

In terms of Laplace transforms:

$$I_{xx}^{O}s^2\Theta(s) + 2k(l_1^2 + l_2^2)\,\Theta(s) = M_i \cdot \frac{1}{s^2}$$

$$I_{xx}^{O}s^2\Theta(s) + k_{eq}\,\Theta(s) = M_i \cdot \frac{1}{s^2}$$

$$\frac{s^2}{\omega_n^2}\Theta(s) + \Theta(s) = \Theta_{fin} \cdot \frac{1}{s^2}$$

The Transfer Function is:

$$T.F. = \frac{\Theta}{\Theta_{fin}} = \frac{1}{s^2} \cdot \frac{\omega_n^2}{\omega_n^2 + s^2}$$

The typical response is [5]:

$$\ddot{\vartheta}(t) = \begin{cases} \dfrac{t - t_0}{t_1 - t_0} - \dfrac{\sin(t - t_0)\omega_n}{(t_1 - t_0)\omega_n} & for\ \ t_0 \le t < t_1 \\ 1 - \cos\left(\dfrac{2t - t_1 - t_0}{\omega_n}\right) \cdot \dfrac{\sin\dfrac{t_1 - t_0}{2}\omega_n}{\dfrac{t_1 - t_0}{2}\omega_n} & for\ \ t \ge t_1 \end{cases}$$

The graphic response is shown in Figure 5.7.

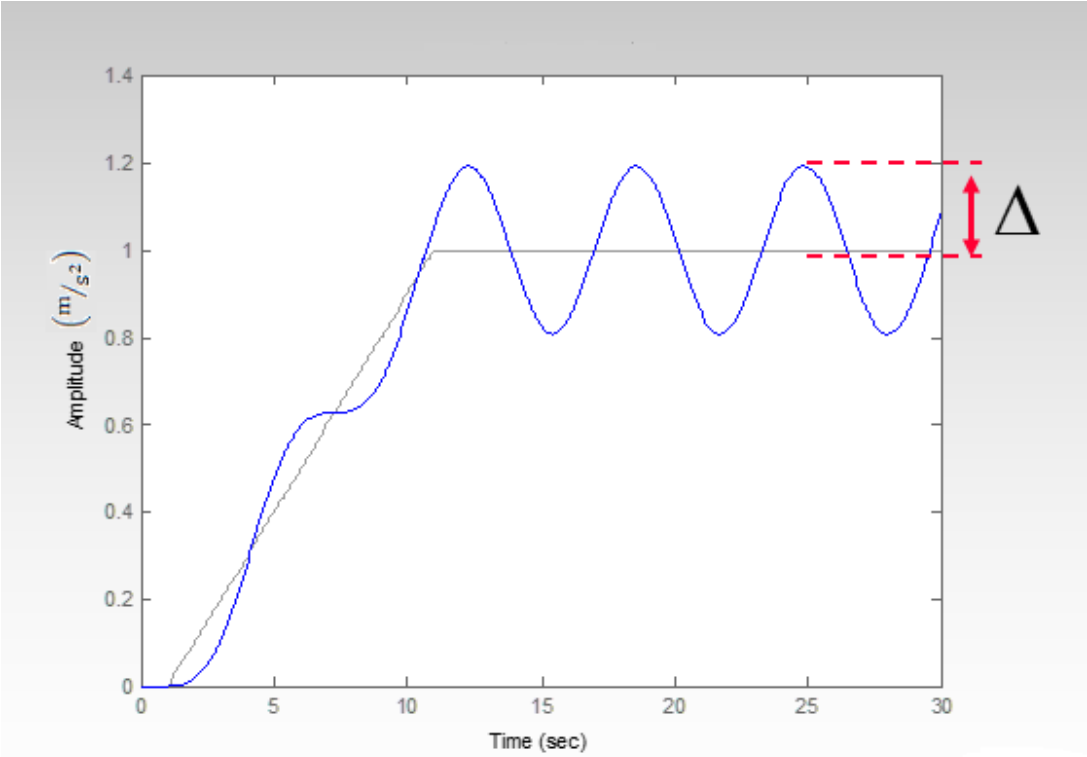


***Figure 5.6**: System response to a linear ramp input of acceleration* [5].

The linear acceleration part is shorter than constant acceleration part. Assuming $t > t_1$:

$$\ddot{\vartheta}(t) = \ddot{\vartheta}_{in}\left[1 - \cos(t - t_1)\omega_n \cdot \mathrm{sinc}\frac{t_1}{2}\omega_n\right]$$

The difference $|\Delta(t)|$ between the input and the output is

$$|\Delta(t)| = \left|\ddot{\vartheta}(t) - \ddot{\vartheta}_{in}\right| = \left|\cos(t - t_1)\omega_n \cdot \mathrm{sinc}\frac{t_1}{2}\omega_n\right| \cdot \ddot{\vartheta}_{in} < \ddot{\vartheta}_{in}$$

$|\Delta(t)|$ is proportional to the factor $sinc\left(\frac{t_1}{2}\omega_n\right) = \frac{\sin\left(\frac{t_1}{2}\omega_n\right)}{\frac{t_1}{2}\omega_n}$

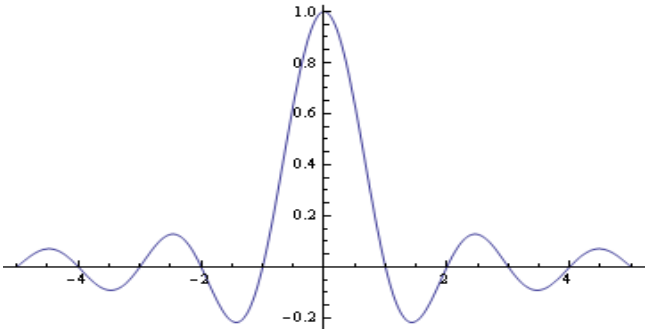


***Figure 5.7**: y=sinc(x).*

The amplitude of the acceleration of the system output corresponding to a linear ramp input is always inferior to the one corresponding to a of step input, and this generates an attenuation of the amplitude:

$$\ddot{\vartheta}(t) = \ddot{\vartheta}_{fin} + \Delta(t) < 2\,\ddot{\vartheta}_{fin}$$

However, at the same performances the introduction of the linear ramp input of acceleration requires an higher input of acceleration, as shown in the Figure 5.9.
Let us consider two symmetric laws of the motion that cover the same distance in the same period $T$, but with two different acceleration profiles.

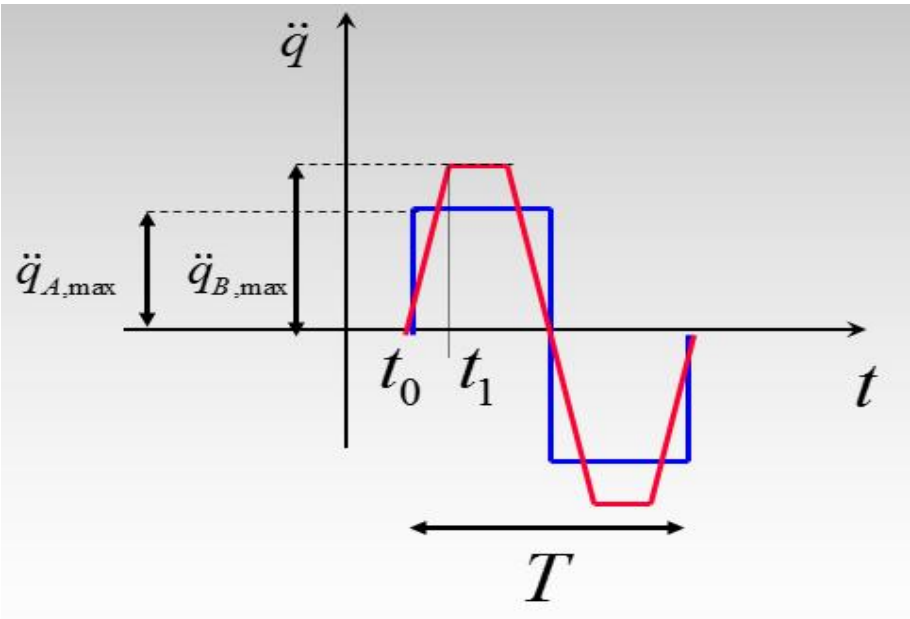


***Figure 5.8****: Two laws of the motion that travel the same distance in the same period, but with two different acceleration profiles. Blue profile is step input; Red profile is linear ramp input* [5].

At the instant $\bar{t} = t_0 + \frac{T}{2}$ the velocities have the same value because of the symmetry of the profiles:

$$\dot{q}_{A,\bar{t}} = \dot{q}_{B,\bar{t}} \quad \rightarrow \quad \ddot{q}_{A,max} \cdot \frac{T}{2} = \ddot{q}_{B,max} \cdot \frac{T-2(t_1-t_0)}{2} \quad \rightarrow \quad \frac{\ddot{q}_{A,max}}{\ddot{q}_{B,max}} = \frac{1}{1-2\frac{t_1-t_0}{T}}$$

The peaks of acceleration of the output are:

$A_{max} = 2\ \ddot{q}_{A,max}$ for the step input profile,

$B_{max} = \ddot{q}_{B,max}(1 + sinc\ \tau\omega_n)$ for the linear ramp input profile, with $\tau = \frac{t_1-t_0}{2}$.

The profile of linear ramp input of acceleration is convenient if the maximum value of acceleration of the corresponding output is lower than the one corresponding to the step input, i.e. if the inequality $A_{max} > B_{max}$ is verified.

$$2\ \ddot{q}_{A,max} > \ddot{q}_{B,max}(1 + sinc\ \tau\omega_n) \quad \rightarrow \quad 1 - 8\frac{\tau}{T} > sinc\ \tau\omega_n$$

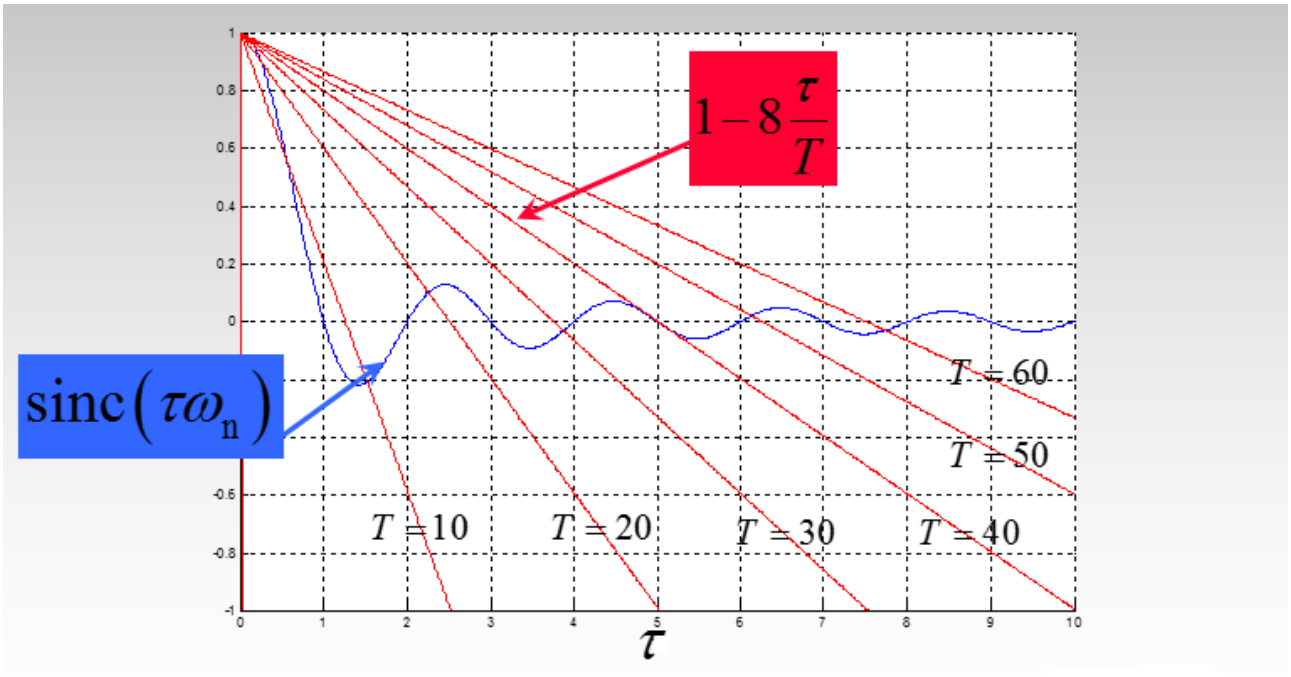


***Figure 5.9**: Representation of the inequality*.

This profile of acceleration is convenient when the duration $T$ of the motion is long, such as $T > 10$ s.

Vibrations caused by inertia forces generate big displacements of the end effector of the manipulators. Two different inputs of acceleration are analysed and compared but in both the durations of the accelerating and braking phases are small in order to complete the motion in a short time and to best exploit the potential of the motor groups.

The worst-case scenario is verified when the step input of acceleration is applied because it generates overshoot up to twice of the static deflection. Moreover, the damping is very small, thus the order of magnitude of the settling time is ten seconds.

Even the application of a ramp input of acceleration does not guarantee a stable behaviour of the system, but it reduces the overshoot although the deflections of the isolation system still represent a problem.

In order to solve these problems, different solutions are possible.

It is demonstrated that the reduction of the discontinuities of the profile of acceleration leads to a reduction of the amplitude of the vibrational phenomena. The use of a profile of acceleration without discontinuities surely helps containing stability oscillation problems during transient motions, although it goes to the detriment of the duration of the motion.

Another option is to introduce a clamping system on the platform that blocks its displacements for all the duration of the transient motion. A solenoid actuator activates the clamping system only during the accelerating and braking phases, stiffening the mobile robot. In these phases, the

system is more vulnerable to vibrations but the duration of transient motions can be considerably reduced thus making the movements faster. When the mobile robot reaches the constant velocity expected by its law of motion, the clamping system is deactivated and the isolation system is free to operate, attenuating the vibration levels on the mobile robot.

The clamping system is useful also when the platform is stopped and the manipulators are moving. Inertia effects produced by their motion generate oscillations of the sprung part of the mobile robot causing loss of accuracy and precision.

Stiffening the platform avoids these oscillations and allows the manipulators to work as they are bolted on a rigid platform.

# 6. Clamping system

In this chapter, the toggle mechanism is described and analysed. Kineto-static simulations are performed using the software “Programa d’Analisi de Mecanismes” (PAM) to design the actuator that activates the mechanism. The steps of PAM are reported in the Appendix 2.

## 6.1. Description of the mechanism

As said at the end the fifth chapter, there is the necessity to introduce a mechanism system that blocks the displacements of the platform during the accelerating and braking phases, and allows the manipulators to work in the best way when the platform is stopped.

Stiffening the system during the accelerating and braking phases makes the mobile robot more vulnerable to vibrations for a short period, but it prevents huge displacements of the end effectors of the manipulators thus enhancing the stability of the system.

A solution available is to introduce in the mobile robot four toggle mechanisms that clamp the two platforms in which the isolators are arranged to limit the vibrations during the transient motion.

This mechanism is commonly used in many applications in which it is required to overcome a large resistance, as the inertia forces of the mobile robot, with a small driving force that can be applied by linear actuator. It is usually adopted for examples in punching, forging and injection moulding machines.

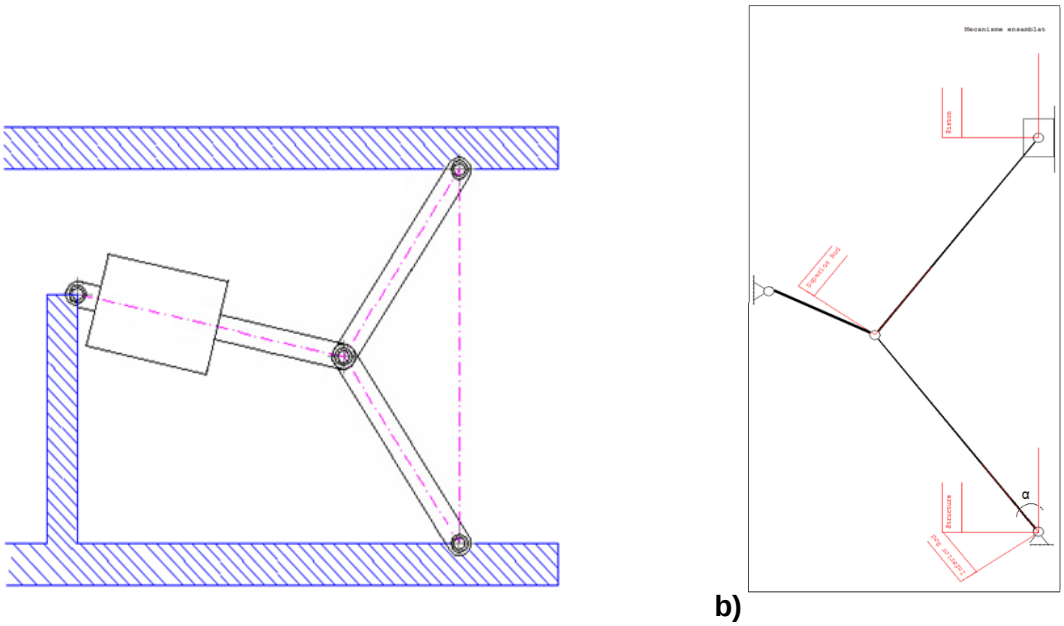

**a)** **b)**

***Figure 6.1a**: Toggle mechanism. The inferior platform is fixed and the upper one is free to move vertically.*
***Figure 6.1b**: A simplified model with piston linked to the upper platform by prismatic joint*.

Two rods and a linear actuator compose this mechanism. The working configuration is near the dead point in which the force required to overcome the resistance is very small. The working cycle of the actuator is of the on/off type and it operates for a very short period until the mechanism is secured in a stable position over the dead point configuration.

Four mechanisms are introduced, one per isolator, in a square configuration between the two platforms. The global displacement of the upper platform is vertical, thus the theoretical model is simplified introducing a piston with prismatic joint at the end of the superior rod that only allows the vertical movement.

The behaviour of the mechanism is analysed using “Programa d’Analisi de Mecanismes” (PAM). With this software, different kinds of mechanisms are simulated doing kinematics and kineto-statics analysis, plotting graphics and exporting all required data.

## 6.2. Results of the kineto-static simulation

Kineto-static simulations show the relation between the actuator force and the angle α, and the angle depends on the geometry. The mechanism moves from the initial configuration with positive angle $\alpha = 10°$ to the final configuration with negative angle $\alpha = -5°$ through the dead point configuration with angle $\alpha = 0°$. The transmission of the force is not stable for α tending to zero, thus this allows to overcome the resistance with small driving force applied by the linear actuator. Graph 6.1 represents the relation between the actuator force and the angle $\alpha$ obtained by kineto-static simulations.

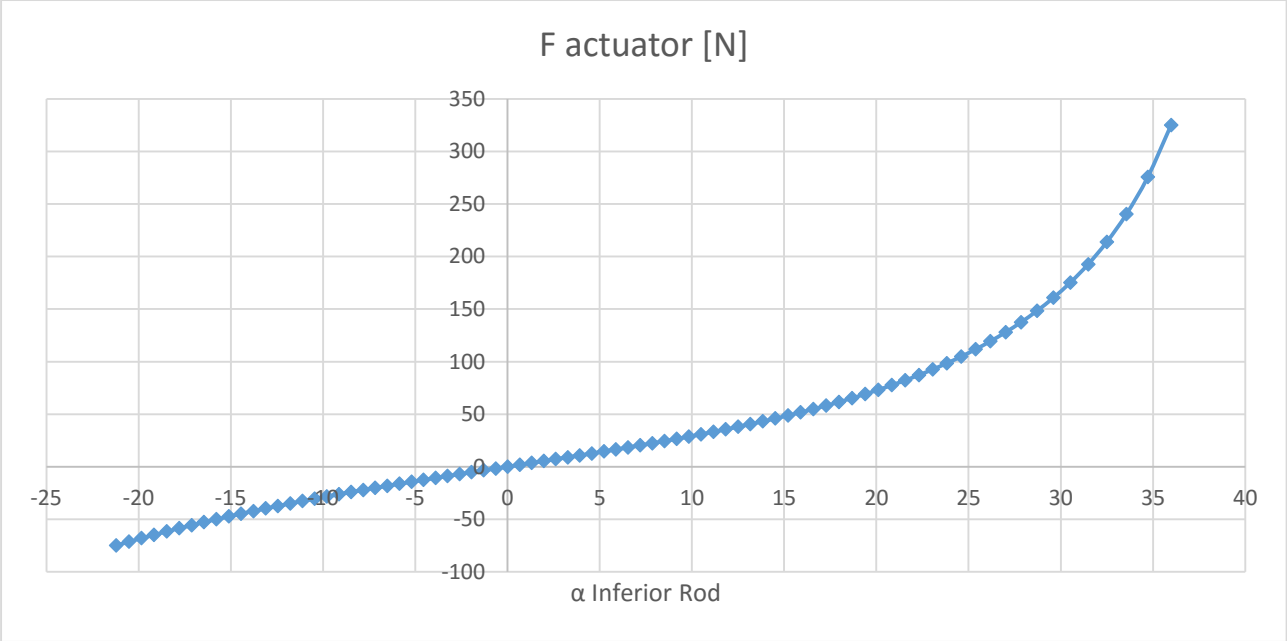


***Graph 6.1**: Relation between the actuator force and the angle $\alpha$ obtained by kineto-static simulations with PAM.*

The angle range more favourable is when α takes values near zero, namely $-5° < \alpha < 10°$. Moreover the direction of the actuator is optimal, i.e. perpendicular to the two rods, when $\alpha = 0°$. The transmission of the force tends to infinity for α tending to 45° because the linear actuator and the Inferior Rod are aligned, thus the action of the actuator is to compress the Inferior Rod.

Zooming Graph 6.1 in the interval $-5° < \alpha < 10°$, it is possible to estimate the force values required by the linear actuator to overcome the resistance.

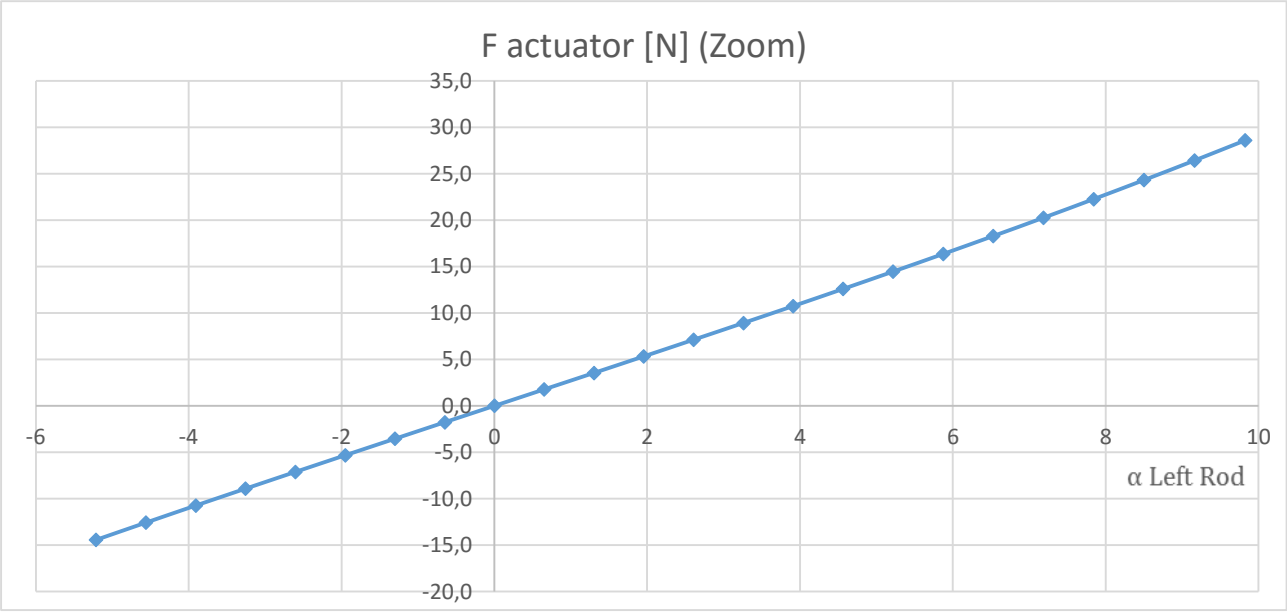


***Graph 6.2**: Detail of Graph 6.1. Only the part of the graph for $-5° < \alpha < 10°$ is displayed.*

The maximum pushing/pulling forces required by the actuator are:

Maximum pushing force: $F_{push} = 28{,}9\ \mathrm{N}$.

Maximum pulling force: $F_{pull} = 14{,}4\ \mathrm{N}$.

The actuator chosen is Linear Solenoid 123422-032 size 2EC from Ledex.

The stroke is approximately $5\ \mathrm{mm}$ and the duty cycle considered is 100% because it is activated only to bring the mechanism in the stable configuration for $\alpha = -5°$.

In the following page, the principal dimensions of the actuator and the graph of the force are reported.

Linear Solenoid 123422-032 size 2EC.

***Figure 6.2**: Linear solenoid*.

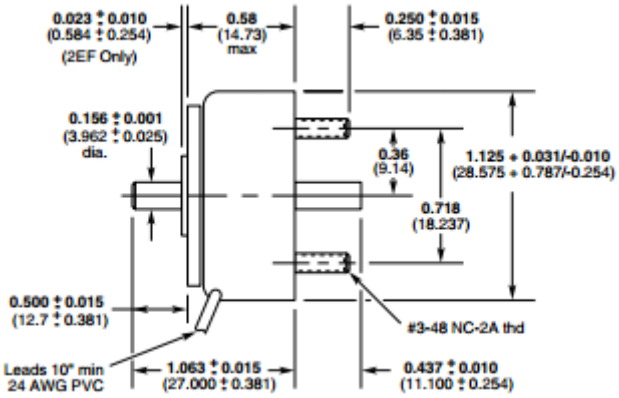


***Figure 6.3**: Drafting of the linear solenoid.*

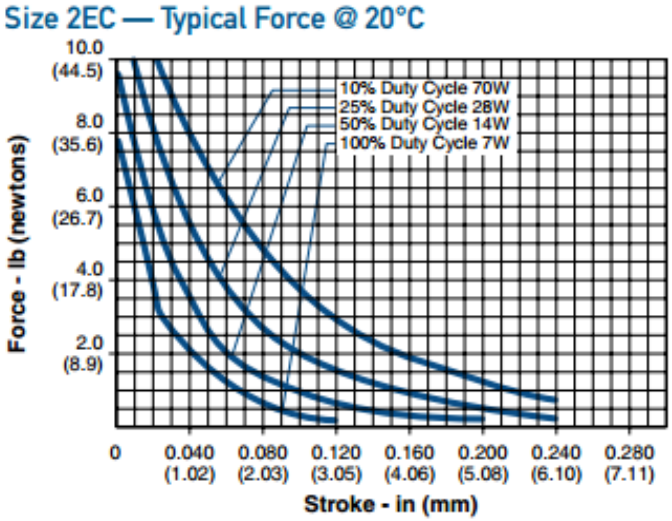


***Figure 6.4**: Representation of the typical force of the actuator.*

# 7. Validation of the theoretical model

In this chapter the validation of the theoretical model is developed. It consists in the comparison of the theoretical results with the results obtained via the execution of laboratory tests that aim to analyse the behaviour of the mobile robot equipped with the isolation system.
Experimental measurements are lead to estimate the real Transmissibility and Attenuation Factor obtained with the introduction of the isolation system. The results are showed and discussed.

## 7.1. Architecture of the mobile robot

The mobile robot used for the validation of the model is the first prototype of mobile robot produced at “Institut d’Organitzaciò i Control”. The elements that compose it are the circular platform provided with omnidirectional wheels and one manipulator by Kuka bolted on the centre of the platform. Figure 5.1 shows the prototype used for the tests.

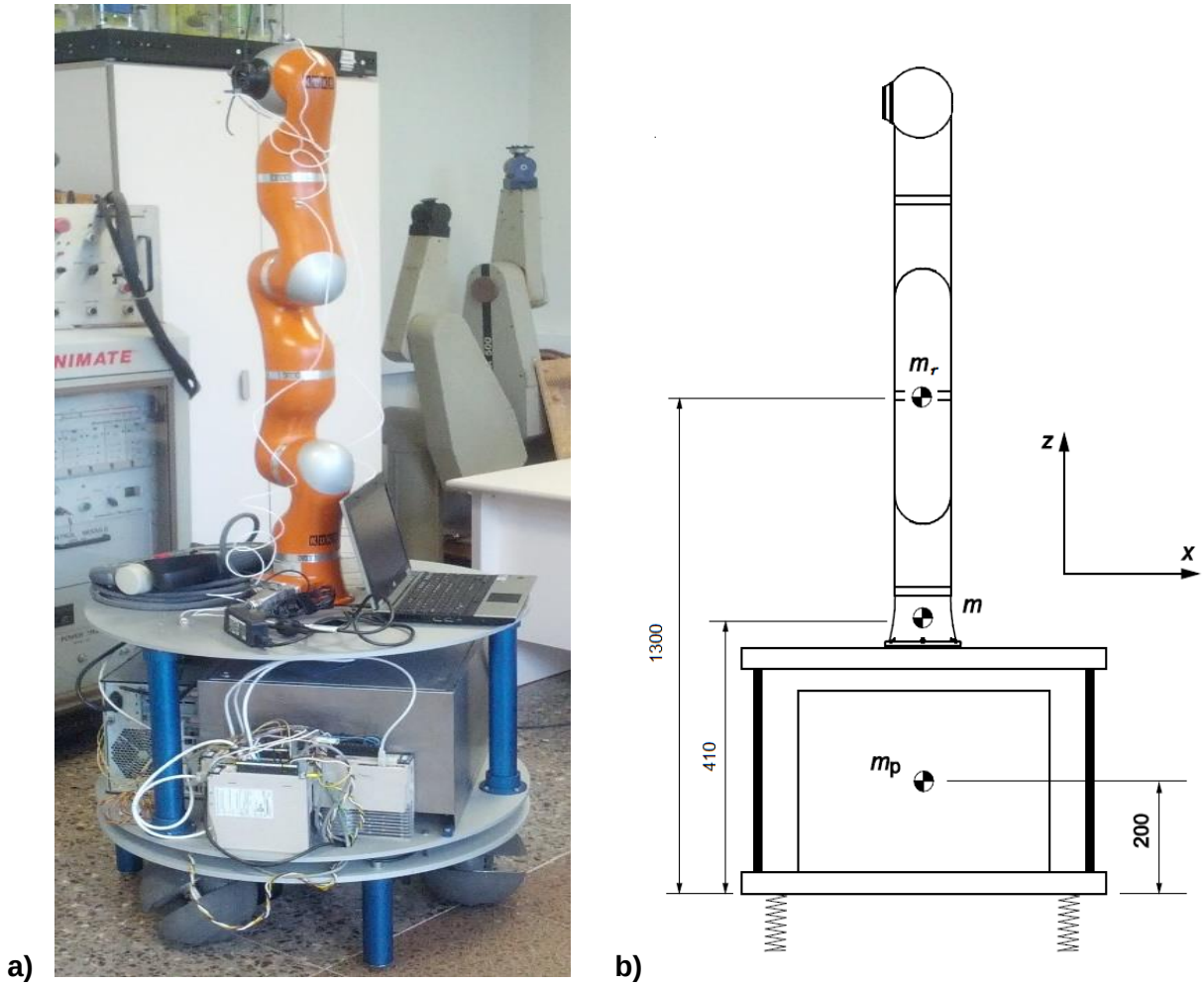


***Figure 7.1a**: First prototype used for the validation of the theoretical model.*
***Figure 7.1b**: Schematic draft of the mobile robot.*

The difference between the new mobile robot and the original one consists in the arrangement of the Kuka robot arm in place of the 'T-shape' frame and the two UR5 manipulators.
This architecture is surely more compact, its inertia moment and mass are inferior than the new mobile robot, but the use of only one manipulator instead of two reduces its capabilities. In particular, the tasks it can achieve, such as pick and place operations, are easier than the complex manipulations made by the cooperation of the arms.
Both mobile robots have to satisfy the same technical specifications given in the first chapter of the project and they are provided with the same platform described in Chapter 1.2.1.

### 7.1.1. Kuka Lightweight Robot 4

The first prototype of mobile robot produced at IOC is provided with a Kuka manipulator.
The Lightweight Robot 4 has a payload capacity of 7 kg. With its in-built sensitivity, achieved by means of the integrated sensors, the LWR 4 is ideally suitable to handling and assembly tasks.
Due to its low weight of 16 kg, the robot is extremely energy-efficient and portable and can thus be used for a wide range of different tasks.

***Figure 7.2**: Kuka Lightweight 4.*

### 7.1.2. Position of the gravity centre

The masses of the elements are:

Platform (*p*) $m_p = 67\ \text{kg}$

Manipulator (*m*) $m_m = 16\ \text{kg}$

Total mass: $m = m_p + m_m = 83\ \text{kg}$.

The distances between the base of the platform and each inertia centre are:

$d_p = 200\ \text{mm}$,

$d_m = 1300\ \text{mm}$.

The position of the global gravity centre is:

$$m\ h = m_p d_p + m_m d_m$$

$$h = \frac{m_p d_p + m_m d_m}{m} = \frac{67 \cdot 200 + 16 \cdot 1300}{83} = 410\ \text{mm}$$

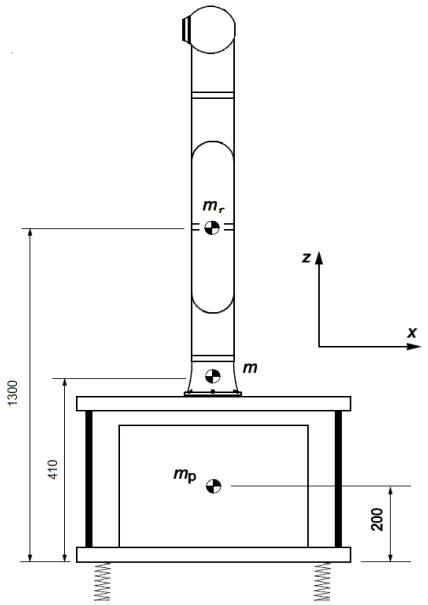


***Figure 7.3**: Configuration used to evaluate the gravity centre and the inertia moment of the mobile robot.*

### 7.1.3. Estimation of the inertia moment

The inertia moments of the mobile robot can be calculated by regarding the members that compose it as cylinders. According to the reference system in Figure 5.2, the platform and the manipulator are z-axis oriented cylinders.
The inertia moment of the two members referred to their own gravity centres are:

Platform: $I_{x,p}^G = I_{y,p}^G = 7\ \mathrm{kgm}^2$,

Manipulator: $I_{x,m}^G = I_{y,m}^G = \frac{1}{12} m_m (3r^2 + l^2) = 1{,}94\mathrm{kgm}^2$.

With $r = 74\ \mathrm{mm}$ and $l = 1200\ \mathrm{mm}$.

The inertia moment of the whole system referred to the global gravity centre is calculated using the Huygens-Steiner theorem. $\delta$ is the distance between member's gravity centre and system's gravity centre. In particular:
$\delta_p = 210\ \mathrm{mm}$,
$\delta_m = 890\ \mathrm{mm}$.

The inertia moment around x-axis $I_x^G$ and y-axis $I_y^G$ are:

$$I_y^G = I_x^G = I_{x,p}^G + m_p \delta_p^2 + I_{x,m}^G + m_m \delta_m^2 = 24{,}6\ \mathrm{kgm}^2$$

## 7.2. Theoretical results

The model that describes the behaviour of the mobile robot is presented in Chapter 4. The two degrees of freedom are the vertical displacement $z$ along z-axis and the pitch rotation $\vartheta$ of the platform around the y-axis according to Figure 7.3.

The graphic representation of the model is shown in Figure 5.3.

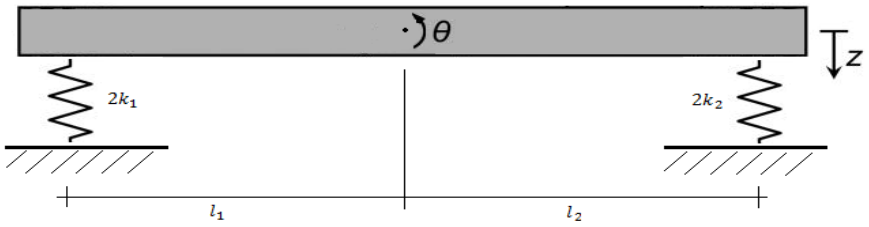


***Figure 7.4**: representation of the model with two degrees of freedom.*

The solution adopted in the first prototype is the same adopted in the new mobile robot. Four isolators of type PLM1 arranged in a square are introduced on the platform. The two degrees of freedom are uncoupled and the matrix representation of the equations of the motion is:

$$\begin{bmatrix} m & 0 \\ 0 & I_y^G \end{bmatrix} \begin{pmatrix} \ddot{z} \\ \ddot{\vartheta} \end{pmatrix} + \begin{bmatrix} 4k & 0 \\ 0 & 4k\,l^2 \end{bmatrix} \begin{pmatrix} z \\ \vartheta \end{pmatrix} = \begin{pmatrix} 0 \\ 0 \end{pmatrix}$$

With:

$k = 6{,}8\,\frac{\mathrm{N}}{\mathrm{mm}}$,

$m = 83\ \mathrm{kg}$,

$I_y^G = 24{,}6\ \mathrm{kgm}^2$,

$l = 235\ \mathrm{mm}$.

Assuming the variables in the following formulation:

$$z = z_0 \sin(\omega_n t) \qquad \dot{z} = \omega_n z_0 \cos(\omega_n t) \qquad \ddot{z} = -\omega_n^2 z_0 \sin(\omega_n t)$$

$$\vartheta = \vartheta_0 \sin(\omega_n t) \qquad \dot{\vartheta} = \omega_n \vartheta_0 \cos(\omega_n t) \qquad \ddot{\vartheta} = -\omega_n^2 \vartheta_0 \sin(\omega_n t)$$

The matrix representation becomes:

$$-\omega_n^2 \begin{bmatrix} m & 0 \\ 0 & I_y^G \end{bmatrix} \begin{pmatrix} z_0 \\ \vartheta_0 \end{pmatrix} \sin \omega_n t + \begin{bmatrix} 4k & 0 \\ 0 & 4kl^2 \end{bmatrix} \begin{pmatrix} z_0 \\ \vartheta_0 \end{pmatrix} \sin \omega_n t = \begin{pmatrix} 0 \\ 0 \end{pmatrix}$$

$$\begin{bmatrix} 4k - \omega_n^2\, m & 0 \\ 0 & 4kl^2 - \omega_n^2 I_y^G \end{bmatrix} \begin{pmatrix} z_0 \\ \vartheta_0 \end{pmatrix} = \begin{pmatrix} 0 \\ 0 \end{pmatrix}$$

The natural frequencies are the solutions of the characteristic equation obtained by equating to zero the determinant of the previous matrix:

$$(4k - \omega_n^2\, m) \cdot \left(4kl^2 - \omega_n^2 I_y^G\right) = 0$$

The two theoretical natural frequencies are:

- For the first degree of freedom:

$$f_{n1,th} = \frac{1}{2\pi}\omega_{n1} = \frac{1}{2\pi}\sqrt{\frac{4\,k}{m}} = \frac{1}{2\pi}\cdot\sqrt{\frac{4 \cdot 6800}{83}} = 2{,}9\ \text{Hz}$$

- For the second degree of freedom:

$$f_{n2,th} = \frac{1}{2\pi}\omega_{n2} = \frac{1}{2\pi}\sqrt{\frac{4\,k\,l^2}{I_y^G}} = \frac{1}{2\pi}\cdot\sqrt{\frac{4 \cdot 6800 \cdot 0{,}24^2}{24{,}56}} = 1{,}3\ \text{Hz}$$

## 7.3. Experimental measurements

The experimental tests were conducted in the laboratory of the Mechanical Engineering Department under the monitoring of operators and supervisors.

The aim is to evaluate the behaviour of the mobile robot with and without the isolation system, estimate the main frequencies that characterize the mobile robot during its motion and analyse in which configuration the vibration level is higher.

Being an UR5 manipulator, the Kuka manipulator's joints are provided with internal brakes that allow to block all the joints for security reason when the robot arm is not powered. When powered, brakes are not active and the electric motor controls the position of the joints.

The presence of the brakes changes the stiffness of the joints and generates different responses of the mobile robot, thus another goal of the experimental tests is to evaluate the differences in term of vibrational response when the manipulator joint's brakes are active or not.

The tests without the isolation system were led in different dates: On 26$^{th}$ February experimental measurements were made with the manipulator's joints braked, and on 4$^{th}$ March with manipulator's joints powered. The tests with the isolation system were led on 15$^{th}$ March with manipulators' joints braked and powered.

### 7.3.1. Configurations

Three configurations of the manipulator, shown in Figure 5.4, were tested. The configuration a) and c) are symmetrical with respect to the xz-plane, according to the reference system reported in Figure 5.1, with the manipulator in vertical position and horizontal longitudinal position. Configuration b) is asymmetrical with the manipulator in horizontal transversal direction with respect to the direction of the motion.

The mobile robot is provided with omnidirectional wheels and the motion is controlled by a personal computer forward and backward along the longitudinal x-axis direction.

**a)**

**b)**

**c)**


***Figure 7.5a**: Horizontal longitudinal position*
***Figure 7.5b**: Horizontal transversal position*
***Figure 7.5c**: Vertical position*

### 7.3.2. Laboratory equipment

The laboratory equipment is the same as the previous measurements, i.e. the two accelerometers B&K and Endevco, placed on the end effector of the manipulator acquiring the acceleration signals in two different directions, and the acquisition system Dewe-43 which they are connected to.

| | | |
|---|---|---|
| Accelerometers: | Brüel&Kjær type 4508 | sensitivity: 9,985 |
| | Endevco type 7254 A-10 | sensitivity: 1,016 |

Acquisition system: Dewe – 43


***Figure 7.6**: End effector with accelerometers.*

In each configuration, one accelerometer is always placed along the vertical direction, the other one in the horizontal longitudinal or transversal direction with respect to the direction of the motion.
Horizontal longitudinal direction is parallel to the direction of the motion.
Horizontal transversal direction is perpendicular to the direction of the motion.
The position and the direction of the accelerometers are reported in the schedule of the tests.

### 7.3.3. Schedule of the tests

The schedule of the tests without the isolation system is:

- 26th February. Platform without isolators. Robot motors braked.

| | |
|---|---|
| Vertical configuration: | B&K vertical position.<br>Endevco horizontal longitudinal position. |
| Vertical configuration: | B&K vertical position.<br>Endevco horizontal transversal position. |
| Horizontal longitudinal configuration: | B&K horizontal transversal position.<br>Endevco vertical position. |
| Horizontal transversal configuration: | B&K horizontal longitudinal position.<br>Endevco vertical position. |

- 4th March. Platform without isolators. Robot motors powered.

| | |
|---|---|
| Vertical configuration: | B&K vertical position.<br>Endevco horizontal longitudinal position. |
| Vertical configuration: | B&K vertical position.<br>Endevco horizontal transversal position. |
| Horizontal longitudinal configuration: | B&K vertical position.<br>Endevco horizontal transversal position. |
| Horizontal transversal configuration: | B&K vertical position.<br>Endevco horizontal longitudinal position. |

Three tests are made for each configuration.

The schedule of the tests with the isolation system is:

- 15th March. Platform with isolators. Robot motors braked.

| | |
|---|---|
| Vertical configuration: | B&K vertical position.<br>Endevco horizontal longitudinal position. |
| Vertical configuration: | B&K vertical position.<br>Endevco horizontal transversal position. |
| Horizontal longitudinal configuration: | B&K vertical position.<br>Endevco horizontal transversal position. |
| Horizontal transversal configuration: | B&K vertical position.<br>Endevco horizontal longitudinal position. |

- 15th March. Platform with isolators. Robot motors powered.

| | |
|---|---|
| Vertical configuration: | B&K vertical position.<br>Endevco horizontal longitudinal position. |
| Vertical configuration: | B&K vertical position.<br>Endevco horizontal transversal position. |
| Horizontal longitudinal configuration: | B&K vertical position.<br>Endevco horizontal transversal position. |
| Horizontal transversal configuration: | B&K vertical position.<br>Endevco horizontal longitudinal position. |

Two tests are made for each configuration.

## 7.4. Results of the data elaboration

The procedure adopted for the data elaboration is the same presented in Chapter 2.

The two signals, filtered and integrated by the acquisition system, are introduced in the software DaDiSP and their power frequency spectra are evaluated for each test. The frequencies with the highest amplitude are considered as the main frequencies that compose the spectra and are collected in Excel for the analysis. The average is calculated between the tests of the same configuration and the results are collected in the Table 7.1.

***Table 7.1a**: Results of tests without isolators and manipulator's joints braked.*

| Joints Braked Without Isolators | $f_{V\ hor}$ [Hz] | Amplitude $f_{V\ hor}$ $\left[\frac{\mathrm{mm}^2}{\mathrm{s}^2}\right]$ | $f_{V\ vert}$ [Hz] | Amplitude $f_{V\ vert}$ $\left[\frac{\mathrm{mm}^2}{\mathrm{s}^2}\right]$ |
|---|---|---|---|---|
| Vertical Longitudinal | 7,2 | 20,2 | 7,0 | 642 |
| Vertical Transversal | 6,9 | 7,9 | 7,1 | 1934 |
| Horizontal Longitudinal | 8,3 | 1068 | 9,4 | 427 |
| Horizontal Transversal | 8,4 | 2476 | 9,2 | 411 |

***Table 7.1b**: Results of tests without isolators and manipulator's joints powered.*

| Joints Powered Without Isolators | $f_{V\ hor}$ [Hz] | Amplitude $f_{V\ hor}$ $\left[\frac{\mathrm{mm}^2}{\mathrm{s}^2}\right]$ | $f_{V\ vert}$ [Hz] | Amplitude $f_{V\ vert}$ $\left[\frac{\mathrm{mm}^2}{\mathrm{s}^2}\right]$ |
|---|---|---|---|---|
| Vertical Longitudinal | 3,9 | 16,9 | 17,8 | 12,2 |
| Vertical Transversal | 7,2 | 1113 | 17,7 | 8,3 |
| Horizontal Longitudinal | 9,9 | 33,0 | 9,6 | 81,5 |
| Horizontal Transversal | 9,4 | 19,2 | 7,8 | 28,5 |

***Table 7.1c**: Results of the tests with isolators and manipulator's joints braked.*

| Joints Braked With Isolators | $f_{V\ hor}$ [Hz] | Amplitude $f_{V\ hor}$ $\left[\frac{\mathrm{mm}^2}{\mathrm{s}^2}\right]$ | $f_{V\ vert}$ [Hz] | Amplitude $f_{V\ vert}$ $\left[\frac{\mathrm{mm}^2}{\mathrm{s}^2}\right]$ |
|---|---|---|---|---|
| Vertical Longitudinal | 7,0 | 16,5 | 3,5 | 45,1 |
| Vertical Transversal | 7,7 | 11,7 | 4,0 | 178,5 |
| Horizontal Longitudinal | 4,3 | 37,8 | 4,8 | 22,6 |
| Horizontal Transversal | 4,4 | 251 | 5,0 | 17,0 |

***Table 7.1d**: Results of the tests with isolators and manipulator's joints powered.*

| Joints Powered With Isolators | $f_{V\ hor}$ [Hz] | Amplitude $f_{V\ hor}$ $\left[\frac{\mathrm{mm}^2}{\mathrm{s}^2}\right]$ | $f_{V\ vert}$ [Hz] | Amplitude $f_{V\ vert}$ $\left[\frac{\mathrm{mm}^2}{\mathrm{s}^2}\right]$ |
|---|---|---|---|---|
| Vertical Longitudinal | 7,9 | 11,3 | 3,0 | 15,5 |
| Vertical Transversal | 7,7 | 12,0 | 4,0 | 49,5 |
| Horizontal Longitudinal | 4,1 | 32,9 | 4,0 | 7,1 |
| Horizontal Transversal | 4,0 | 66,1 | 4,0 | 16,5 |

Comparing the results, several considerations emerge.
They are influenced by the configuration and the state of the joints.

The results of the tests without isolators and with joints braked are presented in Table 5.1a and discussed.
In the Vertical configuration, the frequencies of the Vertical velocity are $7\ \mathrm{Hz}$ with an amplitude of $642\ mm^2/_{s^2}$ and $1934\ \mathrm{mm}^2/_{\mathrm{s}^2}$; the frequencies of the Horizontal Longitudinal and Horizontal Transversal velocities are $7\ \mathrm{Hz}$ with an amplitude of $20\ \mathrm{mm}^2/_{\mathrm{s}^2}$ and $8\ \mathrm{mm}^2/_{\mathrm{s}^2}$ respectively.
In the Horizontal Longitudinal configuration, the frequency of the Vertical velocity is $9{,}4\ \mathrm{Hz}$ with an amplitude of $427\ \mathrm{mm}^2/_{\mathrm{s}^2}$; the frequency of the Horizontal Transversal velocity is $8{,}3\ \mathrm{Hz}$ with an amplitude of $1068\ \mathrm{mm}^2/_{\mathrm{s}^2}$.
In the Horizontal Transversal configuration, the frequency of the Vertical velocity is $9{,}2\ \mathrm{Hz}$ with an amplitude of $411\ \mathrm{mm}^2/_{\mathrm{s}^2}$; the frequency of the Horizontal Longitudinal velocity is $8{,}4\ \mathrm{Hz}$ with an amplitude of $2476\ \mathrm{mm}^2/_{\mathrm{s}^2}$.

The results of the tests without isolators and with joints powered are presented in Table 5.1b and discussed.
In the Vertical configuration, the frequencies of the Vertical velocity is $17{,}8\mathrm{Hz}$ with an amplitude of $12{,}2\ \mathrm{mm}^2/_{\mathrm{s}^2}$; the frequency of the Horizontal Longitudinal velocity is $3{,}9\ \mathrm{Hz}$ with an amplitude of $16{,}9\ \mathrm{mm}^2/_{\mathrm{s}^2}$; the frequency of the Horizontal Transversal velocity is $7{,}2\ \mathrm{Hz}$ with an amplitude of $1113\ \mathrm{mm}^2/_{\mathrm{s}^2}$.
In the Horizontal Longitudinal configuration, the frequency of the Vertical velocity is approximately $9{,}6\ \mathrm{Hz}$ with an amplitude of $81{,}5\ \mathrm{mm}^2/_{\mathrm{s}^2}$; the frequency of the Horizontal Transversal velocity is $9{,}9\ \mathrm{Hz}$ with an amplitude of $33\ \mathrm{mm}^2/_{\mathrm{s}^2}$.
In the Horizontal Transversal configuration, the frequency of the Vertical velocity is $7{,}8\ \mathrm{Hz}$ with an amplitude of $28{,}5\ \mathrm{mm}^2/_{\mathrm{s}^2}$; the frequency of the horizontal longitudinal velocity is $9{,}4\ \mathrm{Hz}$ with an amplitude of $19{,}2\ \mathrm{mm}^2/_{\mathrm{s}^2}$.

As shown, the influence of the state of the joints on the results is very important.
The activation of joints' brakes stiffens the manipulator, thus the sprung mass can be considered mainly as a rigid body. This is more appropriate for the theoretical model.
When joints are powered, i.e. when the position of the members is hold by the motors, the joints' stiffness depends on the motors' torque and generally decreases, thus the hypothesis that the sprung mass is a rigid body vacillates.
In this situation the theoretical model does not describe with sufficient accuracy the behaviour of the mobile robot. Considering the limited stiffness of the joints when powered, the manipulator is no more considerable as a rigid body, the joints should be identified as torsional springs and more degrees of freedom should be introduced in the theoretical model in order to better estimate the behaviour of the mobile robot.
Moreover, the electric motors of the joints are provided with a closed loop control that has to stabilize the position of the joints and try to maintain them static. The motors' torques and consequently joints' stiffness are variable and this prevents an accurate forecast of the torque of the joints of the manipulator.
Once the isolators are introduced on the platform, the influence of the state of the joints is limited and the frequencies of the signals do not change significantly. The amplitude of the vibration are partially reduced and this suggests that the isolation system is working in the proper way.

The results of the tests with isolators and joints braked are presented in Table 5.1c and discussed.
In the Vertical configuration, the frequencies of the Vertical velocity is approximately $3{,}5\,\mathrm{Hz}$ with an amplitude of $45{,}1\ {}^{\mathrm{mm}^2}/_{\mathrm{s}^2}$ and $178{,}5\ {}^{\mathrm{mm}^2}/_{\mathrm{s}^2}$ respectively; the frequencies of the Horizontal Longitudinal and the Horizontal Transversal velocity are approximately $7\,\mathrm{Hz}$ with an amplitude of $16{,}5\ {}^{\mathrm{mm}^2}/_{\mathrm{s}^2}$ and $11{,}7\ {}^{\mathrm{mm}^2}/_{\mathrm{s}^2}$ respectively.
In the Horizontal Longitudinal configuration, the frequency of the Vertical velocity is $4{,}8\,\mathrm{Hz}$ with an amplitude of $22{,}6\ {}^{\mathrm{mm}^2}/_{\mathrm{s}^2}$; the frequency of the Horizontal Transversal velocity is $4{,}3\,\mathrm{Hz}$ with an amplitude of $37{,}8\ {}^{\mathrm{mm}^2}/_{\mathrm{s}^2}$.
In the Horizontal Transversal configuration, the frequency of the Vertical velocity is $5\,\mathrm{Hz}$ with an amplitude of $17\ {}^{\mathrm{mm}^2}/_{\mathrm{s}^2}$; the frequency of the Horizontal Longitudinal velocity is $4{,}4\,\mathrm{Hz}$ with an amplitude of $251\ {}^{\mathrm{mm}^2}/_{\mathrm{s}^2}$.

The results of the tests with isolators and joints powered are presented in Table 5.1d and discussed.

In the Vertical configuration, the frequencies of the Vertical velocity approximately $3{,}5\,\mathrm{Hz}$ with an amplitude of $15{,}5\ {}^{\mathrm{mm}^2}/_{\mathrm{s}^2}$ and $49{,}5\ {}^{\mathrm{mm}^2}/_{\mathrm{s}^2}$ respectively, the frequencies of the Horizontal Longitudinal and the Horizontal Transversal velocity are $7{,}8\,\mathrm{Hz}$ with an amplitude of $11{,}3\ {}^{\mathrm{mm}^2}/_{\mathrm{s}^2}$ and $12\ {}^{\mathrm{mm}^2}/_{\mathrm{s}^2}$ respectively.
In the Horizontal Longitudinal configuration, the frequency of the Vertical velocity is $4\,\mathrm{Hz}$ with an amplitude of $7{,}1\ {}^{\mathrm{mm}^2}/_{\mathrm{s}^2}$; the frequency of the Horizontal Transversal velocity is $4\,\mathrm{Hz}$ with an amplitude of $32{,}9\ {}^{\mathrm{mm}^2}/_{\mathrm{s}^2}$.
In the Horizontal Transversal configuration, the frequency of the Vertical velocity is $4\,\mathrm{Hz}$ with an amplitude of $16{,}5\ {}^{\mathrm{mm}^2}/_{\mathrm{s}^2}$; the frequency of the Horizontal Longitudinal velocity is $4\,\mathrm{Hz}$ with an amplitude of $66{,}1\ {}^{\mathrm{mm}^2}/_{\mathrm{s}^2}$.

As expected from the theoretical model, the introduction of the isolation system reduced significantly the vibration levels of the mobile robot up to 90% in the case of the Vertical velocity in the Vertical configuration. The end effector of the mobile robot oscillates at the low frequency of $4\,\mathrm{Hz}$. The low natural frequencies of the mobile robot allow to better isolate the system from low frequency disturbances.

The Transmissibility *T* describes how much of the input is transferred to the output; the Attenuation Factor *A.F.* defines the attenuation that the isolation system provides to the mobile robot.
They are mutually related through the following formulations expressed in percentage:

$$T = \frac{\sqrt{1+\left(2\xi\frac{f}{f_n}\right)^2}}{\sqrt{\left(1-\frac{f^2}{f_n{}^2}\right)^2+\left(2\xi\frac{f}{f_n}\right)^2}} \quad [\%] \qquad\qquad A.F. = 1 - T \quad [\%]$$

The parameters involved are:
$f$ is the frequency of the external disturbance estimated from the tests without the isolation system, $f_n$ is the natural frequency of the mobile robot estimated from the tests with the isolation system in case of the real Transmissibility or from the theoretical model in case of the Theoretical Transmissibility.

The input has a wide frequency spectrum, thus the frequency at which the input has spectrum has its highest amplitude is close to the natural frequency of the mobile robot, according to the

experimental tests led without the isolation system, and they depend on the particular configuration and joints' state. That frequency is considered as the frequency of the external disturbance that afflicts the mobile robot during its motion to be isolated.
The Theoretical Transmissibility $T_{th}$ is evaluated using the frequency of the external disturbance and the natural frequency obtained by the theoretical model. It is analytically calculated only for the Vertical velocity of the Vertical configuration.
The real Transmissibility is evaluated using the frequency of the external disturbance and the natural frequency obtained by the experimental measurements with the isolation system. It is calculated for the Vertical and Horizontal velocities in each configuration.
The comparison defines the validity of the theoretical model.

In Table 5.2 the values of the Transmissibility and Attenuation Factor are shown related to the frequency of the Vertical velocity in the two different joints' state.

***Table 7.2a**: Values of Transmissibility and Attenuation Factor with manipulator's joints braked.*

| $f_{V\ vert}$ Configuration | $T$ [%] | $T_{th}$ [%] | $A.F.$ [%] | $A.F_{th}$ [%] |
|---|---|---|---|---|
| Vertical Longitudinal | 5,65 | 4,27 | 94,35 | 95,73 |
| Vertical Transversal | 7,17 | 4,30 | 92,83 | 95,70 |
| Horizontal longitudinal | 23,16 | | 76,84 | |
| Horizontal Transversal | 42,50 | | 57,50 | |

***Table 7.2b**: Values of Transmissibility and Attenuation Factor with manipulator's joints powered.*

| $f_{V\ vert}$ Configuration | $T$ [%] | $T_{th}$ [%] | $A.F.$ [%] | $A.F_{th}$ [%] |
|---|---|---|---|---|
| Vertical Longitudinal | 35,59 | 22,55 | 64,41 | 77,45 |
| Vertical Transversal | 34,05 | 21,68 | 65,95 | 78,32 |
| Horizontal longitudinal | 18,01 | | 81,99 | |
| Horizontal Transversal | 18,87 | | 81,13 | |

Table 5.2a shows the values of the Transmissibility and Attenuation Factor with manipulator's joints braked. The values of the Real Attenuation Factor and the Theoretical Attenuation Factor are compatible within a reduced margin of error of 5%. The theoretical model describes very well the behaviour of the mobile robot in this particular configuration and joints' state. The solution introduced on the platform gives excellent results.

Table 5.2b shows the values of the Transmissibility and Attenuation Factor with manipulator's joints powered. The values of the Real Attenuation Factor and the Theoretical Attenuation Factor are compatible within a reduced margin of error of 15%. The theoretical model is less accurate than in the previous case due to the state of the joints of the manipulator, but it provides an acceptable estimate of the attenuation of the isolation system.

The solution designed for the new mobile robot is introduced and tested on the first prototype built to verify the precision of the theoretical model. It gives globally accurate results that can be extended to the new mobile robot, which the solution is designed for.
In particular, when the joints are braked the results of the comparison are surely encouraging, while when the joints are powered the theoretical results are a good estimate within a margin of error of 15%.
The theoretical model ensures that the introduction of the isolation system on the platform of the new mobile robot will give good results. Moreover the solution proposed is designed specifically for it so the effects of the isolation system are enhanced.

# Conclusions

In this thesis, the topic of passive vibrations isolation applied to a mobile robot has been discussed. After a short presentation of the mobile robot and the description of its architecture, experimental measurements were made to estimate the natural frequencies of the mobile robot and the wide frequency spectrum of the disturbance. Two configurations were tested to understand in which one the vibration level is higher.

Then, the theoretical model with two degrees of freedom was implemented to estimate the stiffness of the isolation system. The number and the arrangement of the isolators were chosen in order to uncouple the degrees of freedom. Four pneumatic isolators by Fabreeka were finally acquired.

Special attention was paid to the stability of the mobile robot during the transient motion due to the introduction of the isolation system. Different profiles of acceleration were studied and compared considering the effects of the discontinuities of the acceleration profile on the dynamic of the mobile robot.

The introduction of a clamping system that blocks the deflections of the isolators during transient motions enhanced the stability of the mobile robot and helped reduce the displacements caused by inertia forces. Kineto-static simulations were run in order to design the actuator that activates the mechanism.

In the last part of the project, the precision of the theoretical model was verified by experimental measurements. The solution proposed was introduced in the previous prototype of mobile robot testing several configurations and joints' states. Experimental Transmissibility and Attenuation Factor were evaluated and compared with theoretical results.

Theoretical results ensured the good attenuation of the vibrational phenomena and globally accurate results during its motion, thus the theoretical model could be applied to the new mobile robot, which the solution was designed for.

The results of the comparison were encouraging in particular with joints braked, ensuring a margin of error between 5 and 15%.

Finally, environment impact and budget evaluation were discussed.

# Appendix 1

In this appendix, the instrumentations that compose the laboratory equipment are described.

## Endevco Model 7254 A10

The Endevco Model 7254 A10 is a small and rugged piezoelectric accelerometer with integral electronics, designed for measuring vibrations on structures and objects. The unit is hermetically sealed to prevent environmental contamination. It features high output sensitivity, high signal-to-noise ratio, and wide bandwidth. This accelerometer incorporates an internal hybrid signal conditioner in a two-wire system, which transmits its low impedance voltage output through the same cable that supplies the constant current power.

***Figure A1.1**: Endevco Model 7254 A10*

## Brüel & Kjær type 4508

The Brüel & Kjær type 4508 is specifically designed to withstand the rough environment of the automotive industry. A combination of high sensitivity, low mass and small physical dimensions make them ideal for modal measurements. The slotted cylindrical stanchion holds a central seismic mass flanked by two piezoelectric plates. This assembly is clamped rigidly by a ring and is hermetically welded to the titanium housing. The parts are firmly held together without the use of any bonding agent other than friction, a principle which has proved reliable in Brüel & Kjær DeltaShear accelerometers.

***Figure A1.2**: Brüel & Kjær type 4508.*

## Data acquisition system Dewe-43

When connected to the high speed USB 2.0 interface of any computer the Dewe-43 becomes a powerful measurement instrument for analog, digital, counter and CAN-bus data capture.

Eight simultaneous analog inputs sample data in combination with Dewetron Modular Smart Interface modules (MSI) a wide range of sensors are supported such as Voltage, Acceleration, Pressure, Force, Temperature, Sound, Position RPM, Torque, Frequency and Velocity. Each analog inputs has its own sigma-delta A/D converter and is sampled at up to 204,8 kS/s at 24-bit resolution.

Anti-aliasing filters are included for each channel and all are our “universal” type, which can handle full bridges and voltages up to ±10 V natively and support our tiny Modular Smart Interfaces.


***Figure A1.3**: Data acquisition system Dewe-43.*

# Appendix 2

In this appendix, the six steps for assembling and simulating correctly the toggle mechanism are described using the software “Programa d’Analisi de Mecanismes” (PAM).

## Steps for PAM

In PAM different steps have to be to be completed in order to assembly the mechanism in the correct way.

1) In the first step, general characteristics of the mechanism are set. These are the number of members, joints, external forces and actuators that act in the model. Four members compose the toggle mechanism: the fixed structure, two rods and a piston. The structure counts as a member and requires its constraint.

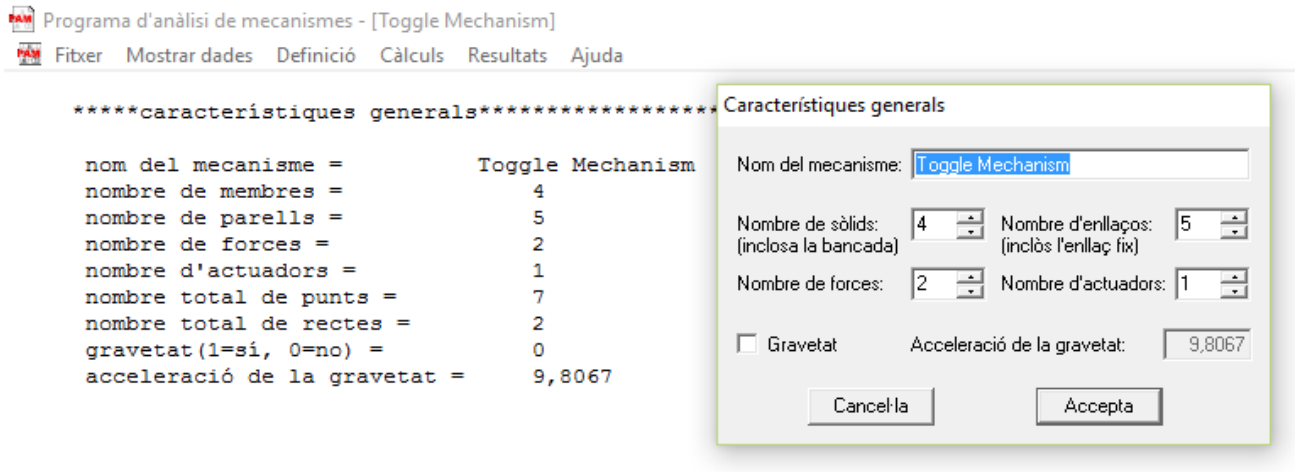


***Figure A2.1**: Screenshot of the first step. Definition of the general characteristic as number of members, joints, forces and actuators.*

2) In the second step, it is required to define for each member how many points and straight lines compose the element.

   One point and one line define the piston: the point represents the position of its gravity centre and the straight line its sliding direction.
   Two points and one line define the frame. One point is linked to the actuator, the other one to the inferior rod. The straight line is the sliding direction of the piston.
   Two points define the two rods. These are the extremity points of the member.

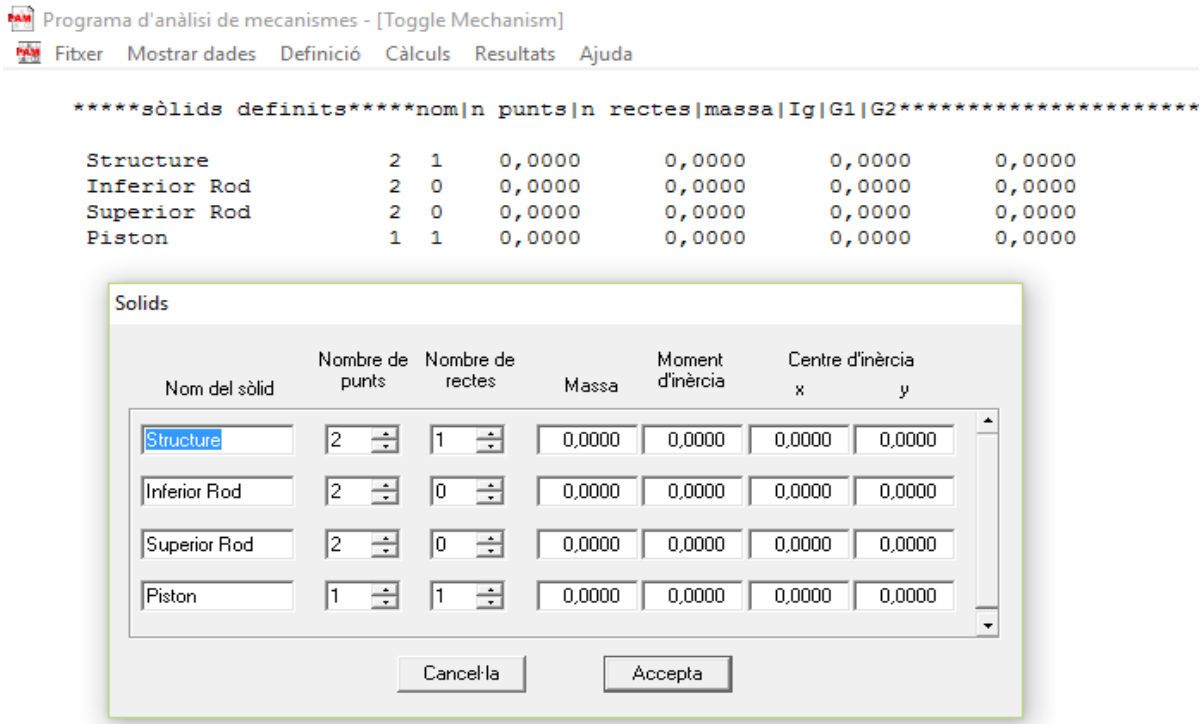


***Figure A2.2**: Screenshot of the second step. Definition of points and straight lines for each member.*

3) In the third step, the geometry of the mechanism is specified: coordinates of points and orientations of lines with respect to their own reference system.

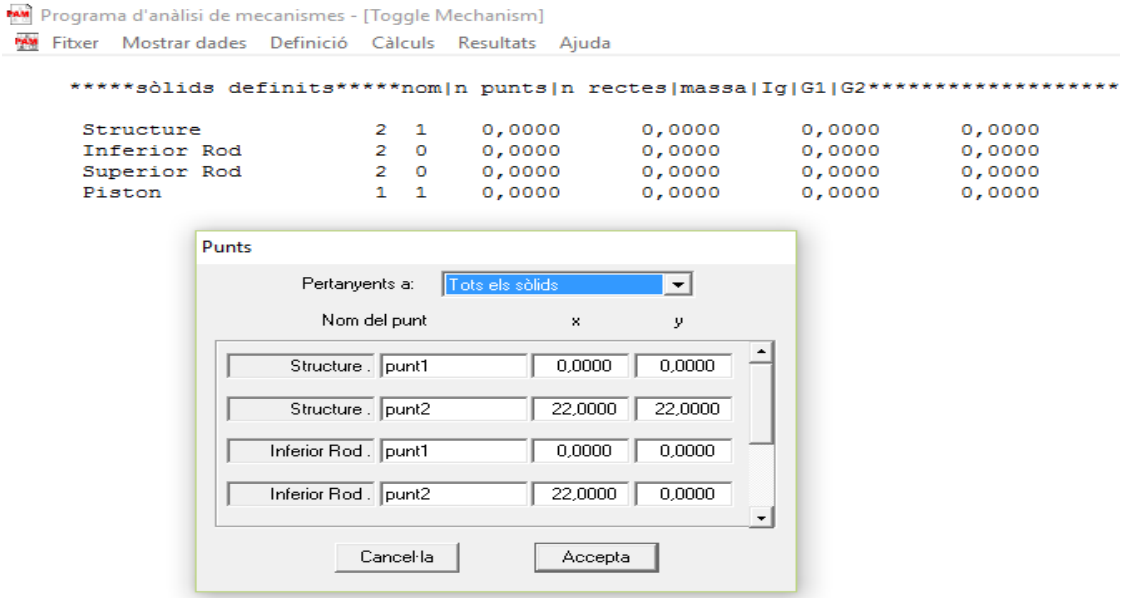


***Figure A2.3**: Screenshot of the third step. Geometric definition of the points of each member.*

The length of each rod is supposed to be 22 millimetres.

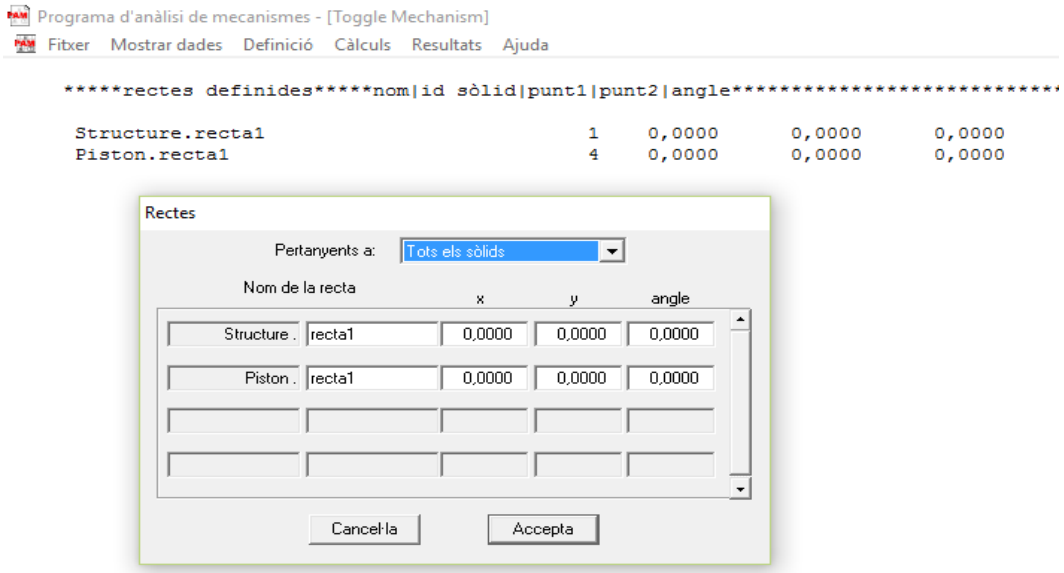


***Figure A2.4****: screenshot of the third step. Geometric definition of the orientation of the straight lines for each member.*

4) In the fourth step, joints between members are defined.

The frame is fixed and linked to the inferior rod by a rotational joint.

The extreme points of the two rods are linked together by a rotational joint.

Piston is linked to the frame by a prismatic joint and to the superior rod by a rotational joint.

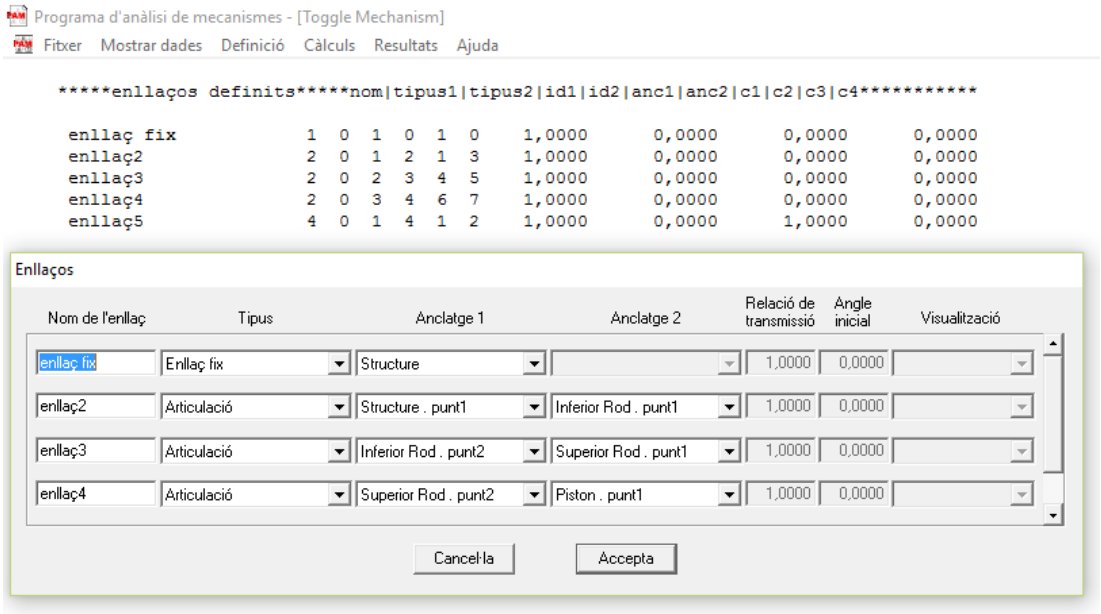


***Figure A2.5****: Screenshot of the fourth step. Definition of the joints that link the members.*

5) In the fifth step, two forces acting in the mechanism are introduced.
    - Inertia force is applied to the piston in vertical direction.
    - Elastic force of the isolator is applied between the piston and the structure.

Inertia force $F_i$ is defined as a constant vector $\overline{F_i} = (F_x; F_y; M_z)$ in the global reference system.
The maximum linear acceleration of the platform $a = 1\,{}^{\mathrm{m}}/_{\mathrm{s}^2}$ is assumed as the most critical situation in order to estimate it.
Inertia force applied to gravity centre of the mobile robot is $F_i = m \cdot a = 128{,}8\ \mathrm{N}$.

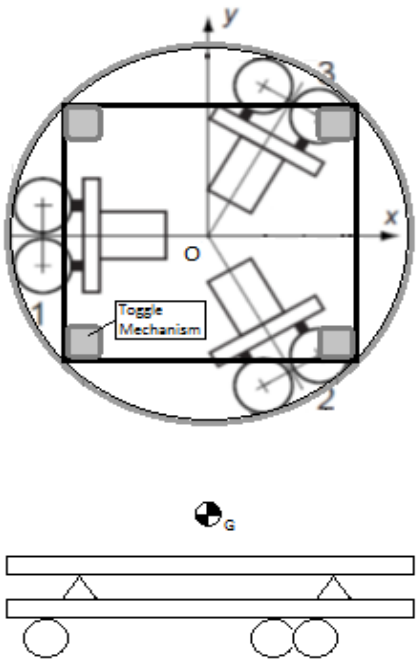


***Figure A2.6**: Positions of motor groups, clamping system, and gravity centre of the mobile robot.*

The gravity centre distances from the rotation axis by $h = 524\ \mathrm{mm}$ thus the pitch momentum is:

$$M_i = F_i\, h = 128{,}8 \cdot 0{,}524 = 67{,}5\ \mathrm{Nm}$$

The symmetric disposition of the system allows to have two supports that react to the pitch moment.
The reaction force of the two supports is:

$$F_R = \frac{M_i}{l_{tot}} = \frac{67{,}5}{0{,}410} = 165\ \mathrm{N}$$

That means each support sustains a reaction force that is ${F_R}/{2} = 82\ \mathrm{N}$ along the vertical direction.

$$\overline{F_i} = \left(0; -\frac{F_R}{2}; 0\right) = (0; -82; 0)$$

Elastic force $F_e$ produced by the isolator acts between two points: the gravity centre of the piston and the structure. It is defined as:

$$F_e = c_1 + c_2(\rho - c_3) + c_4 \cdot \frac{d\rho}{dt} = -6{,}8\ (\rho - 43{,}4)$$

With: $c_1 = 0$ $c_2 = k = -6{,}8\ {}^{\mathrm{N}}/_{\mathrm{mm}}$ $c_3 = \rho_0 = 43{,}4\ \mathrm{mm}$ $c_4 = 0$

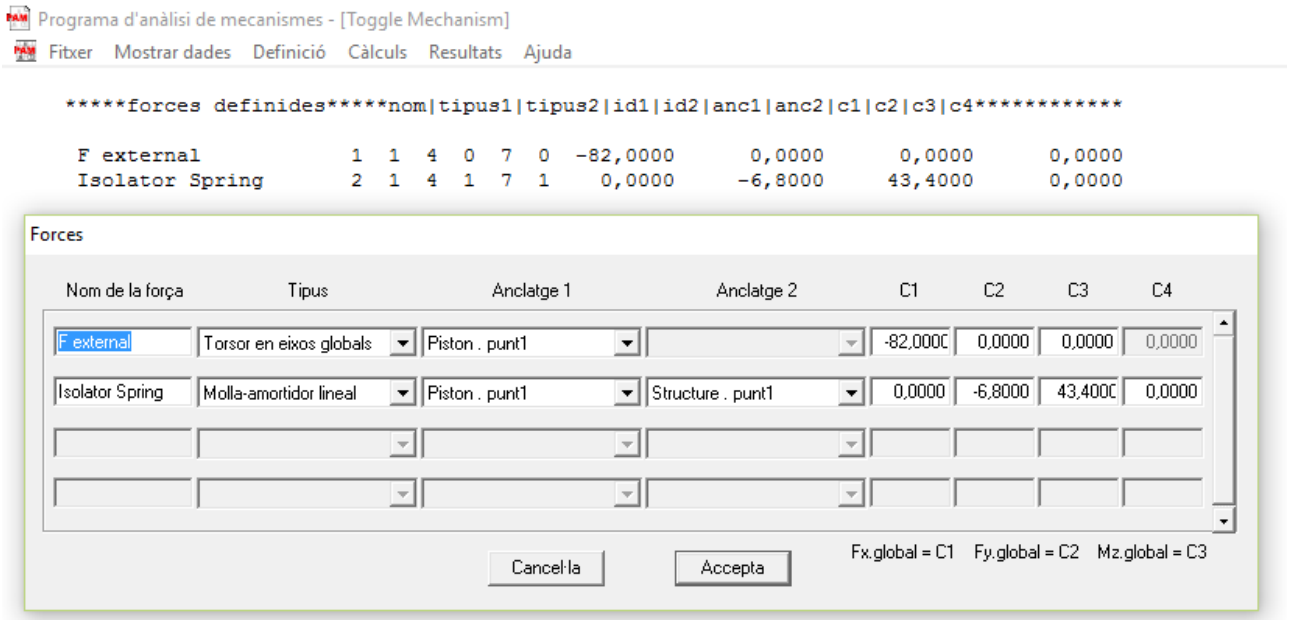


***Figure A2.7**: Screenshot of the fifth step. Definition of the inertia force $F_i$ and the elastic force $F_e$.*

6) In the last step, the position of the actuator is defined. It is placed between the intersection of the two rods and the structure. The temporal law of motion is set, although it is not required.

   The simulation made is a kineto-static one, thus there is no time dependence.

   The law of motion is polynomial and linear affine in the time variable:

$$f(t) = c_1 + c_2 \cdot t + c_3 \cdot t^2 + c_4 \cdot t^3 = 10 + 5 \cdot t$$

With: $c_1 = 10\ \mathrm{mm}$ $c_2 = 5\ {}^{\mathrm{mm}}/_{\mathrm{s}}$ $c_3 = 0$ $c_4 = 0$

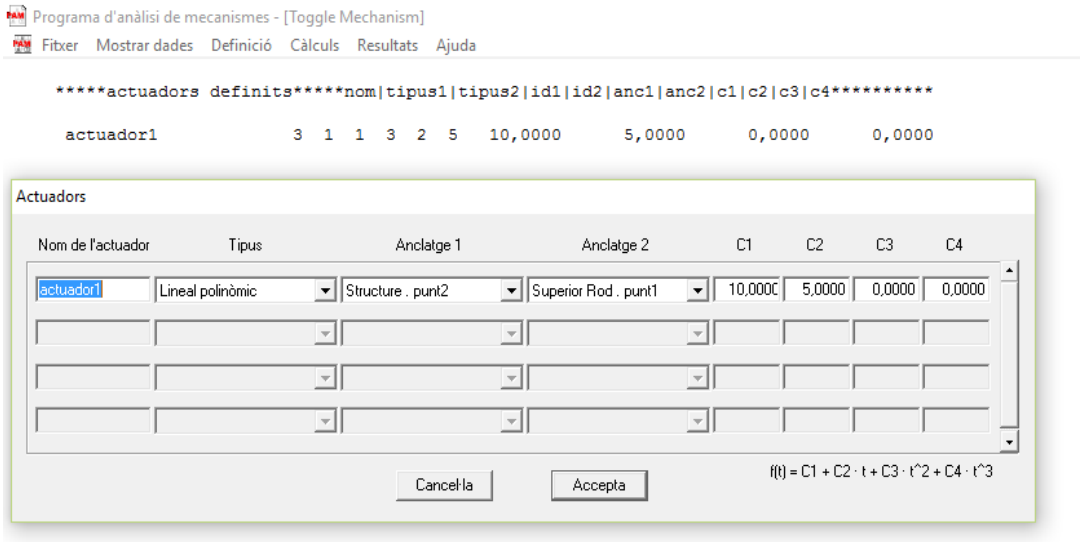


***Figure A2.8**: Screenshot of the sixth step. Definition of actuator's law of motion.*

Once the geometry and the main characteristics of the members are defined, it is possible to assemble the mechanism.

Figure A2.9 shows three configurations of the toggle mechanism: the initial configuration for $\alpha = 10°$, the dead point configuration for $\alpha = 0°$ and the stable configuration for $\alpha = -5°$.

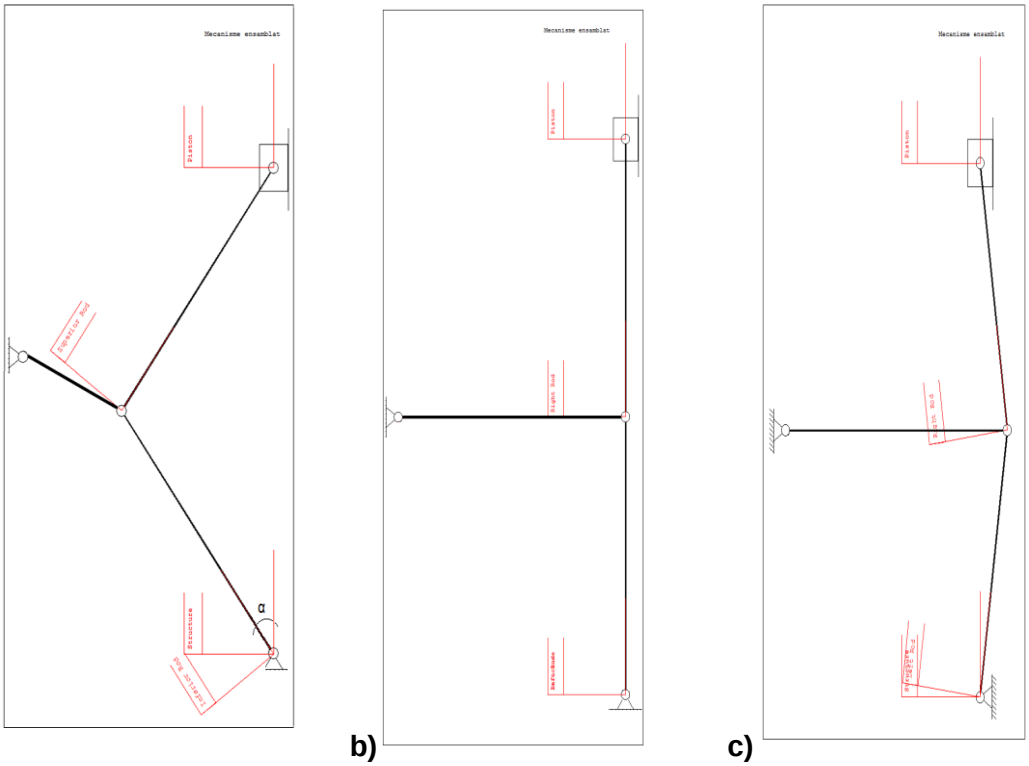


***Figure A2.9a**: Initial configuration for $\alpha = 10°$.*
***Figure A2.9b**: Singular configuration for $\alpha = 0°$.*
***Figure A2.9c**: Final configuration for $\alpha = -5°$.*

# Bibliography


[1] J. Martìnez, D. Costa. Plataforma Mòbil amb Rodes esfèriques per al Robot "Lightweight Robot 4" de Kuka Roboter. Escola Tecnica Superior d'Enginyeria Industrial de Barcelona, 2012.

[2] S. Cardona, L. Jordi. Vibracions Mecàniques, Disseny d'un Aïllamenet Elàstic. Escola Tecnica Superior d'Enginyeria Industrial de Barcelona, 2000.

[3] J.A. Batlle, A. Barjau. Holonomy in Mobile Robots. Robotics and Autonomous Systems 57 (2009) 433-440, 2009.

[4] K. Kufieta. Force Estimation in Robotic Manipulators: Modelling, Simulation and Experiments. PhD thesis, Norwegian University of Science and Technology, NTNU, 2014.

[5] J. Schrimpf. Sensor-based Real-time Control of Industrial Robots. PhD thesis, Norwegian University of Science and Technology, NTNU, 2013.

[6] Klas Kronander, Aude Billard. Learning Compliant Manipulation through Kinesthetic and Tactile Human-Robot Interaction. Escola Tecnica Superior d'Enginyeria Industrial de Barcelona, 2013.

[7] ATI Industrial Automation. Network Force/Torque Sensor System, Compilation of Manuals, February 2013.

[8] J. Gamez Garcia, A. Robertsson, J. Gomez Ortega, and R. Johansson. Sensor for compliant robot motion control. IEEE Transactions on Robotics, 24(2):430–441, 2008.

[9] J.G. Proakis and D.G. Manolakis. Digital Signal Processing: Principles, Algorithms & Applications. Pearson Prentice Hall, fourth edition, 2007.

[10] M. Quigley, R. Brewer, S.P. Soundararaj, V. Pradeep, and A.Y. Ng. Low-cost accelerometers for robotic manipulator perception. 2010 IEEE/RSJ International Conf. on Intelligent Robots and Systems, pages 6168–6174, October 2010.

[11] P. Roan, N. Deshpande, Y. Wang, and B. Pitzer. Manipulator state estimation with low cost accelerometers and gyroscopes. 2012 IEEE/RSJ International Conf. on Intelligent Robots and Systems, pages 4822–4827, October 2012.

[12] Claire Dumas, Stephane Caro, Cherif Mehdi, Sebastien Garnier, Benoit Furet. Joint Stiffness Identification of Industrial Serial Robots. Robotica, Cambridge University Press, 2011, pp.1-20.

[13] B. Siciliano, L. Sciavicco, L. Villani, and G. Oriolo. Robotics: Modelling, Planning & Control. Springer, 2009.

[14] Universal Robots. PolyScope Manual, February 2013.

[15] Universal Robots. The URScript Programming Language, February 2013.

[16] Universal Robots. User Manual: UR5, February 2013.

[17] Fabreeka. Low Frequency Isolation Solution Manual, 2009.

[18] Kuka Roboter GmbH. Lightweight Robot 4 Manual, 2010.